The conserved ATPase PCH-2 controls the number and distribution of crossovers by antagonizing their formation in *C. elegans*

Bhumil Patel, Maryke Grobler, Alberto Herrera, Elias Logari, Valery Ortiz, and Needhi Bhalla[1]

Department of Molecular, Cell and Developmental Biology, University of California, Santa Cruz, Santa Cruz, CA 95064

[1] corresponding author: nbhalla@ucsc.edu
Department of Molecular, Cell and Developmental Biology
225 Sinsheimer Labs
University of California, Santa Cruz
Santa Cruz, CA 95064
phone: (831) 459-1319
fax: (831) 459-3139

Abstract

Meiotic crossover recombination is essential for both accurate chromosome segregation and the generation of new haplotypes for natural selection to act upon. This requirement is known as crossover assurance and is one example of crossover control. While the conserved role of the ATPase, PCH-2, during meiotic prophase has been enigmatic, a universal phenotype when *pch-2* or its orthologs are mutated is a change in the number and distribution of meiotic crossovers. Here, we show that PCH-2 controls the number and distribution of crossovers by antagonizing their formation. This antagonism produces different effects at different stages of meiotic prophase: early in meiotic prophase, PCH-2 prevents double strand breaks from becoming crossover-eligible intermediates, limiting crossover formation at sites of initial double strand break formation and homolog interactions. Later in meiotic prophase, PCH-2 winnows the number of crossover-eligible intermediates, contributing to the designation of crossovers and ultimately, crossover assurance. We also demonstrate that PCH-2 accomplishes this regulation through the meiotic HORMAD, HIM-3. Our data strongly support a model in which PCH-2's conserved role is to remodel meiotic HORMADs throughout meiotic prophase to destabilize crossover-eligible precursors, coordinate meiotic recombination with synapsis, and contribute to the progressive implementation of meiotic recombination, guaranteeing crossover control.

Introduction

Meiosis is a specialized type of cell division that reduces chromosome number by half, resulting in the production of genetically diverse haploid gametes, so that fertilization during sexual reproduction restores diploidy. This process occurs in two stages: meiosis I, in which homologous chromosomes are partitioned, and meiosis II, in which sister chromatid are segregated. The regulation of meiosis is crucial for ensuring that both genetic recombination and chromosome segregation occur accurately. Errors in human meiosis are associated with birth defects, such as Down and Turner syndromes, infertility and miscarriages, underscoring the importance of understanding meiosis to human health (Hassold and Hunt, 2001).

During prophase I, homologous chromosomes pair and this pairing is stabilized through a process called synapsis, in which a protein structure called the synaptonemal complex (SC) holds homologs together. This close association between homologs during synapsis facilitates crossover formation, the process in which double strand breaks (DSBs) are deliberately introduced into the genome, repaired by meiosis-specific mechanisms that exchange DNA between homologous chromosomes and generate the chiasmata, or linkage, that promotes accurate meiotic chromosome segregation. Therefore, disruptions in pairing, synapsis, or recombination prevent the formation of chiasmata and can lead to meiotic errors such as nondisjunction, resulting in aneuploid gametes.

In addition to the fundamental role that recombination plays in ensuring accurate chromosome segregation, crossover recombination accomplishes another important function: it generates new haplotypes for natural selection to act upon to drive evolution. Thus, to assure a random assortment of alleles on a population level, the distribution of crossovers may be as tightly regulated as their number (Veller et al., 2019). The significance of controlling both crossover number and distribution is clearly illustrated by the existence of mechanisms such as crossover assurance, in which every pair of homologous chromosomes gets at least one crossover; crossover homeostasis, in which the number

61 of crossovers remains relatively invariant even if the number of recombination precursors change; and
62 crossover interference, in which the presence of a crossover inhibits the formation of a crossover
63 nearby (Gray and Cohen, 2016). DSBs typically vastly outnumber crossovers in most organisms and
64 are introduced gradually throughout early prophase (Joshi et al., 2015; Woglar and Villeneuve, 2018).
65 Therefore, to accomplish this precise level of control, meiotic crossover recombination and the
66 decision about which DSBs become crossover-eligible intermediates, and eventually, which crossover-
67 eligible intermediates get designated as crossovers, is implemented progressively throughout meiotic
68 prophase (Cole et al., 2012; Joshi et al., 2015; Morgan et al., 2021; Yokoo et al., 2012). In many
69 systems, transitions from DSBs to crossover-eligible intermediates, and crossover-eligible
70 intermediates to crossovers, can be molecularly and/or cytologically monitored.
71
72 PCH-2, also known as TRIP13 in mammals, is an evolutionarily ancient AAA-ATPase that plays a
73 significant role in regulating meiosis across different organisms, including *M. musculus* (mice), *S.*
74 *cerevisiae* (budding yeast), *D. melanogaster* (fruit flies), and *C. elegans* (worms) (Bhalla, 2023). PCH-
75 2 and its orthologs structurally remodel a family of proteins with HORMA domains (HORMADs) to
76 control their function (Gu et al., 2022). HORMADs participate in a variety of signaling events and can
77 exist in at least three structurally distinct conformations: a “closed” conformation, which they adopt
78 when they bind a short peptide sequence in their own protein sequence or another protein (also called
79 a closure motif) and their C-terminus wraps around this motif to stabilize the interaction; an “open”
80 conformation when unbound, in which their C-terminus is discretely tucked against the HORMA
81 domain; and an “extended” conformation, which is an intermediate between the two (Gu et al., 2022).
82 PCH-2 and its orthologs convert the closed version of HORMADs to the open or extended versions,
83 playing an important role in recycling HORMADs during signaling. During meiosis, closed versions of
84 meiotic HORMADs assemble on chromosomes to form meiotic chromosome axes, which are essential
85 for pairing, synapsis and recombination between homologous chromosomes (Kim et al., 2014). The
86 remodeling of meiotic HORMADs by PCH-2 to an “open” or “extended” conformation is thought to
87 reduce the levels of HORMADs on chromosomes (Borner et al., 2008; Cuacos et al., 2021; Lambing

et al., 2015; Wojtasz et al., 2009) and/or increase their dynamic association and dissociation (Russo et al., 2023), modulating and coordinating homolog pairing, synapsis and recombination during prophase.

The conserved role of the PCH-2/HORMAD module in meiosis has been difficult to characterize, in part, we have argued, because of the evolutionary innovation that is an inherent aspect of sexual reproduction (Bhalla, 2023). Moreover, in some systems, such as budding yeast and plants (Herruzo et al., 2021; Yang et al., 2020), PCH-2 orthologs not only remodel meiotic HORMADs on meiotic chromosomes but also perform this function in the cytoplasm to make meiotic HORMADs available for their role(s) in meiotic nuclei. This dual role can complicate functional analyses, particularly in *pch-2* null mutants. However, all meiotic systems exhibit defects in the number and distribution of crossovers when PCH-2 function is abrogated by mutation (Deshong et al., 2014; Joshi et al., 2009; Joyce and McKim, 2009; Lambing et al., 2015; Roig et al., 2010; Zanders and Alani, 2009). Unfortunately, the lack of a clear pattern when analyzing these defects in recombination in *pch-2* mutants has contributed to an inability to develop a unified, integrated model of PCH-2 function in the field.

In *C. elegans*, meiotic HORMADs localize to meiotic chromosomes independently of PCH-2 (Deshong et al., 2014). Moreover, the progressive implementation of meiotic recombination can be cytologically monitored in meiotic nuclei that are organized both spatially and temporally in the *C. elegans* germline (Woglar and Villeneuve, 2018; Yokoo et al., 2012). Here, we exploit this system to show that PCH-2 is required to control the number and distribution of crossovers by antagonizing their formation. This antagonism produces different consequences depending on the stage of meiotic prophase. In early meiotic prophase, PCH-2 inhibits DSBs from becoming crossover-eligible intermediates, ensuring that crossovers are more widely distributed than sites of initial DSB formation and/or homolog interactions. Later in meiotic prophase, PCH-2 is responsible for winnowing the numbers of crossover-eligible intermediates on synapsed chromosomes, contributing to the designation of crossovers and ultimately, crossover assurance. Genetic analysis demonstrates that PCH-2's regulation of crossover-eligible

115 intermediates is through one of three essential meiotic HORMADs, HIM-3. Finally, we link PCH-2's
116 effect on early DSBs in early meiotic prophase to cell cycle stage, demonstrating that both limit early
117 DSBs from becoming crossovers. We propose that PCH-2's remodeling of HIM-3 on meiotic
118 chromosomes destabilizes crossover-eligible intermediates throughout meiotic prophase, contributing
119 to the progressive implementation of meiotic recombination to control the number and distribution of
120 crossovers, also known as crossover control.

121

122 **Results**

123 **PCH-2 controls the number and distribution of crossovers in similar patterns on multiple**
124 **chromosomes**

125

126 We had previously shown that loss of PCH-2 reduced the frequency of double crossovers and genetic
127 length of both an autosome (chromosome III) and the X chromosome, albeit not uniformly among
128 genetic intervals (Deshong et al., 2014). To determine whether a more obvious pattern could be
129 observed, we expanded our analysis by monitoring recombination genetically in both wildtype and
130 *pch-2* mutant animals using five single nucleotide polymorphisms (SNPs) that spanned 95% of
131 Chromosomes, I, III, IV and the X chromosome (Figure 1). We excluded Chromosome II from our
132 analysis because of the potential difficulty combining Hawaiian SNPs with the *pch-2* mutation, which is
133 linked to Chromosome II, and Chromosome V because of our use of the *bcIs39* transgene to identify
134 cross progeny, which may disrupt recombination on that chromosome.

135

136 In wildtype animals, we observed multiple double crossovers, ranging from 1-13, depending on the
137 chromosome. In a majority of these double crossovers (69%), one crossover was at the end of the
138 chromosome where pairing and synapsis initiate, also called the Pairing Center (PC) (MacQueen et
139 al., 2005), suggesting some relationship between where chromosomes might make initial contacts and
140 the likelihood of double crossovers. On all chromosomes analyzed, we observed no double
141 crossovers in *pch-2* mutants and this difference was statistically significant for Chromosomes I, III and

142 X. Moreover, there was a striking and consistent shift of crossovers to the PC end of all four
143 chromosomes tested. This shift in the distribution of crossovers to the PC ends of chromosomes was
144 generally accompanied by a reduction in crossovers in the center of chromosomes. In *C. elegans*, the
145 center of chromosomes are where double strand breaks are less numerous (Nadarajan et al., 2021;
146 Yu et al., 2016) and where genes are more abundant. In the case of the X chromosome and
147 chromosome III, recombination at the non-PC end was also reduced and appeared to more closely
148 resemble the physical map at this end of these chromosomes. Thus, PCH-2 ensures a wider
149 distribution of crossovers across chromosomes, away from regions that are more likely to undergo
150 early homolog interactions (PC ends) and with more double strand breaks (both the PC and non-PC
151 ends of chromosomes), and towards the center of chromosomes, where double strand breaks are less
152 abundant.

153

154 **PCH-2 prevents exogenous DSBs early in meiotic prophase from becoming crossovers**

155

156 We previously showed that PCH-2 promotes crossover formation and crossover assurance through its
157 regulation of the meiotic HORMAD, HIM-3, in *C. elegans* (Russo et al., 2023). Moreover, this
158 promoting role seems linked to its localization to the synaptonemal complex (Patel et al., 2023).
159 However, the observed shift in the distribution of crossovers in *pch-2* mutants suggests that PCH-2
160 may also play a role in inhibiting crossovers and that this role may be occurring in early meiotic
161 prophase, when chromosomes are undergoing initial homolog interactions. We had previously
162 observed that meiotic nuclei in early prophase were more likely to produce crossovers when DSBs
163 were induced by excision of the *Mos* transposon in *pch-2* mutants than in control animals but
164 experimental caveats limited our ability to properly interpret this experiment (Deshong et al., 2014).

165

166 To explicitly test this possibility, we took advantage of both the spatiotemporal organization of meiotic
167 nuclei in the *C. elegans* germline, and the observation that nuclei travel in an assembly line process at
168 a stereotypical pace to late pachytene (Jaramillo-Lambert et al., 2007), where we can cytologically

169 assess crossover formation by staining for the essential crossover factor, COSA-1 (Yokoo et al.,
170 2012). We performed irradiation experiments to introduce exogenous DSBs at different timepoints
171 during meiotic prophase and analyzed PCH-2's role in crossover formation (Figure 2A).

172

173 In this experiment, we tested the effects of ionizing radiation at two distinct time points: 8 hours after
174 irradiation, when we can monitor crossover formation in late pachytene nuclei that received
175 exogenous DSBs in mid-pachytene, and 24 hours after irradiation, when we monitor crossover
176 formation in late pachytene nuclei that received exogenous DSBs in leptotene/zygotene, also known
177 as the transition zone in *C. elegans* (Figure 2A). In order to detect crossovers in late pachytene,
178 control and *pch-2* mutants germlines were stained for GFP::COSA-1, which allowed us to visualize
179 crossovers, and DAPI, which allowed us to visualize DNA. In unirradiated control worms, 94% of late
180 pachytene nuclei have 6 GFP::COSA-1 foci, one per chromosome pair (Figure 2B). In unirradiated
181 *pch-2* mutants, the percentage of nuclei have 6 GFP::COSA-1 foci drops to 82%, primarily because of
182 the significant increase in meiotic nuclei with less than 6 GFP::COSA-1 foci (17%) (Figure 2B),
183 consistent with our previous report that loss of PCH-2 leads to a decrease in crossover formation
184 (Deshong et al., 2014). At 8 hours after irradiation, *pch-2* mutants' defect in crossover assurance
185 becomes even more pronounced. We observed a significant increase in nuclei containing less than 6
186 COSA-1 nuclei in *pch-2* mutants (26%), when compared to control (9%) germlines (Figures 2C and
187 2D). However, we did not observe a significant number of nuclei with greater than 6 COSA-1 foci in
188 either backgrounds. This observation reinforces previous findings that exogenous DSBs introduced in
189 mid-pachytene do not affect the number of crossovers in wildtype animals (Yokoo et al., 2012).

190

191 Next, we examined crossover formation 24 hours post-irradiation (Figures 2E and 2F). For this time
192 point, we also detected a significant loss of crossover assurance in *pch-2* mutants, compared to
193 control worms. However, in contrast to the 8 hour time point, we also saw a significant increase in
194 nuclei containing less than 6 COSA-1 foci in both control (13%) and *pch-2* mutants (26%), compared

195 to unirradiated worms (p values = 0.0008 and < 0.0001, respectively, Fischer's Exact Test), indicating
196 that even in control animals, extra DSBs in early meiotic prophase can disrupt crossover assurance. In
197 addition, we also observed a significant increase in nuclei with more than 6 COSA-1 foci in *pch-2*
198 mutants (wildtype: 2%, *pch-2*: 13%), demonstrating that loss of PCH-2 leads to increased crossover
199 formation when nuclei in the transition zone get more DSBs. In other words, PCH-2 inhibits
200 exogenous DSBs introduced in early meiotic prophase from becoming crossovers, supporting our
201 recombination analysis (Figure 1).
202
203 **PCH-2 prevents SPO-11-induced DSBs from becoming crossovers in early meiotic prophase**
204
205 Our previous experiment indicated that PCH-2 is preventing exogenous DSBs in early meiotic
206 prophase from becoming crossovers (Figure 2). To test whether this was also the case for
207 programmed meiotic DSB formation, we used the auxin-inducible degradation (AID) system to remove
208 the enzyme that is responsible for programmed meiotic DSBs, SPO-11 (*spo-11::AID::3XFLAG*)
209 (Dernburg et al., 1998; Keeney et al., 1997). When we treated both control and *pch-2* mutant worms
210 for 36 hours with auxin (Figure 3A), we observed a complete loss of GFP::COSA-1 foci (Figure 3C).
211 When these animals were treated with auxin for 48 hours, to allow nuclei without SPO-11 an additional
212 12 hours to reach diakinesis (Figure 3D), we observed 12 DAPI stained bodies, or univalents, which
213 are the 6 homolog pairs that have not formed chiasmata (Figure 3F). Thus, we can reliably remove
214 SPO-11 from meiotic nuclei throughout the germline and prevent crossover formation.
215
216 Since meiotic nuclei travel through the germline at about one cell per row per hour (Jaramillo-Lambert
217 et al., 2007), we took advantage of this precise spatiotemporal resolution to test four different
218 timepoints in early meiotic prophase to determine if acute depletion of SPO-11 leads to any changes in
219 crossover formation between control animals and *pch-2* mutants (Figures 3A and D). In this
220 experiment, we assayed crossover formation with two experimental approaches. Similar to our
221 irradiation experiment (Figures 2E and 2F), we assayed crossover formation by analyzing the number

222 of GFP::COSA-1 foci in late pachytene 24, 22, 20 and 18 hours after acutely depleting SPO-11 (Figure
223 3A). In addition to this approach, we analyzed the presence of bivalents in diakinesis (Figure 3D),
224 which indicates the successful formation of chiasmata between homologous chromosomes. Since
225 meiotic nuclei travel from late pachytene to diakinesis in approximately 12 hours (Deshong et al.,
226 2014), the 36, 34, 32 and 30 hour timepoints to assay bivalent formation correspond to the 24, 22, 20
227 and 18 hour timepoints, respectively, in which GFP::COSA-1 were analyzed. We also performed a
228 control experiment, treating worms with ethanol for 24 and 36 hour timepoints to ensure that this
229 tagged version of SPO-11 was fully functional for crossover formation (Figures 3C and 3F).

230

231 At the 24 hour time point (Figures 3A and 3C), when meiotic nuclei in the transition zone do not
232 receive SPO-11-induced DSBs, we observe a range of GFP::COSA-1 foci in late pachytene in both
233 control animals and *pch-2* mutants with a majority of nuclei having 0 or 1 focus (control and *pch-2*
234 averages: 1.8 GFP::COSA-1 foci), indicating a loss of crossover formation, albeit with some
235 heterogeneity. This heterogeneity likely reflects that it takes 1-4 hours to significantly affect DSB
236 formation through acute degradation of SPO-11 at this stage of meiosis in *C. elegans* (Hicks et al.,
237 2022). In addition, there was no statistically significant difference in the number of GFP::COSA-1 foci
238 between control animals and *pch-2* mutants. However, when we assayed bivalent formation 12 hours
239 later (see 36 hours auxin treatment in Figures 3D and 3F), we observed the same heterogeneity and a
240 slight, statistically significant difference in the number of DAPI stained bodies between control animals
241 (average number of DAPI stained bodies: 10.6) and *pch-2* mutants (average number of DAPI stained
242 bodies: 9.6), suggesting that even at this very early time point, we can detect a role for PCH-2 in
243 preventing early SPO-11-induced DSBs from becoming crossovers.

244

245 We continued to monitor GFP::COSA-1 and bivalent formation at successive timepoints. At the 22
246 hour and 34 hour timepoints, where SPO-11 depletion begins later in the transition zone, we saw an
247 increase in the number of GFP::COSA-1 foci (Figure 3C) and a reduction in the number of DAPI

248 stained bodies (Figure 3F), suggesting that more DSBs are becoming crossovers. In our analysis of
249 GFP::COSA-1 foci at this timepoint, there appeared to a bimodal distribution: the majority of nuclei in
250 both genotypes fell into two clear classes, those with no COSA-1 foci (24% in control animals, 26% in
251 *pch-2* mutants) and those with 6 COSA-1 foci (42% in both control animals and *pch-2* mutants)
252 (Figure 3C). The number of crossovers continued to increase at the 20 hour and 32 hour timepoints,
253 eventually reaching wildtype numbers for GFP::COSA-1 and DAPI stained bodies by the 18 hour and
254 30 hour timepoints, respectively (Figures 3C and 3F).
255
256 At the 22 hour and 34 hour timepoints, we did not detect any statistically significant difference in the
257 number of GFP::COSA-1 foci or DAPI stained bodies between control animals and *pch-2* mutants
258 (Figures 3C and 3F), even when we analyzed the number of nuclei that had greater than 6
259 GFP::COSA-1 foci. In contrast, while the number of GFP::COSA-1 foci was not statistically
260 significantly different between control animals and *pch-2* mutants at the 20 hour time point (Figure
261 3C), the number of nuclei with greater than 6 GFP::COSA-1 foci was significantly higher in *pch-2*
262 mutants (control: 3%, *pch-2*: 10%, p value = 0.009, Fischer's Exact Test), similar to our analysis of
263 GFP::COSA-1 24 hours after irradiation. Even more strikingly, the number of DAPI stained bodies was
264 significantly lower in *pch-2* animals than control animals at the corresponding 32 hour timepoint
265 (Figure 3F), indicating that more homolog pairs had successfully formed chiasmata in *pch-2* mutants.
266 No difference in GFP::COSA-1 foci or bivalent formation was observed at the 18 hour and 30 hours
267 timepoints, respectively (Figures 3C and 3F). These data indicate that during a narrow time frame of
268 early meiotic prophase, likely during leptotene/zygotene given the delay in limiting DSB formation with
269 auxin-induced degradation of SPO-11, PCH-2 prevents SPO-11-induced DSBs from becoming
270 crossovers and chiasmata.
271
272 **PCH-2 is required for timely loading and removal of MSH-5 on meiotic chromosomes through**
273 **its regulation of HIM-3**
274

275 After DSB formation, a subset of DSBs are licensed to be repaired through a pro-crossover pathway
276 and eventually winnowed to a stereotypical number of crossovers (Yokoo et al., 2012). In *C. elegans*,
277 these crossover-eligible intermediates can be visualized by the loading of the pro-crossover factor
278 MSH-5, a component of the meiosis-specific MutS γ complex that stabilizes crossover-specific DNA
279 repair intermediates called joint molecules (Janisiw et al., 2018; Kelly et al., 2000; Snowden et al.,
280 2004). In the spatiotemporally organized meiotic nuclei of the germline, a functional GFP tagged
281 version of MSH-5, GFP::MSH-5, begins to form a few foci in leptotene/zygotene (the transition zone),
282 becoming more numerous in early pachytene before decreasing in number in mid pachytene to
283 ultimately colocalize with COSA-1 marked sites in late pachytene in a process called designation
284 (Janisiw et al., 2018; Woglar and Villeneuve, 2018; Yokoo et al., 2012; see control in Figures 4A and
285 4B). The mechanism through which MSH-5 functions with the SC and other meiosis factors to
286 ultimately form crossovers has not been established but may involve phosphorylation by cyclin-
287 dependent kinases (Haversat et al., 2022; Zhang et al., 2021).

288

289 Given that we have shown that PCH-2 prevents early DSBs from becoming crossovers (Figures 2 and
290 3), we tested whether we could cytologically detect this inhibition at the level of MSH-5 behavior in
291 control animals and *pch-2* mutants. We generated wildtype and *pch-2* mutants with GFP::MSH-5 and
292 quantified the average number of GFP::MSH-5 foci per row of nuclei from the transition zone to late
293 pachytene (Figures 4A and 4B). We observed a statistically significant increase in the average number
294 of GFP::MSH-5 foci per row in the transition zone in *pch-2* mutants (Figures 4A and 4B, p value <
295 0.0001, Student's t-test), indicating that PCH-2 typically limits MSH-5 loading at this early stage of
296 meiotic prophase. The average number of GFP::MSH-5 foci per row were similar in number in early
297 pachytene in both backgrounds. However, we also observed a substantial increase in the average
298 number of GFP::MSH-5 foci per row in *pch-2* mutants in the mid and late pachytene regions (Figures
299 4A and 4B), indicating that PCH-2 also promotes the turnover or maturation of GFP::MSH-5 foci at
300 these later stages of meiotic prophase. Thus, PCH-2 prevents the loading of the crossover-promoting

301 factor, MSH-5, limiting the formation of crossover-eligible intermediates during early meiotic prophase,
302 consistent with both our genetic analysis of recombination (Figure 1) and PCH-2's role in preventing
303 early DSBs from becoming crossovers (Figures 2 and 3). However, PCH-2 also appears to limit the
304 number of crossover-eligible intermediates in mid and late pachytene, an unexpected observation
305 given that the most severe recombination defect in *pch-2* mutants is the loss of crossover assurance
306 (Deshong et al., 2014).

307

308 We previously showed that PCH-2 genetically interacts with meiotic HORMADs to control different
309 aspects of meiosis. A mutant version of the essential meiotic HORMAD, HIM-3^{R93Y}, binds its closure
310 motif with reduced affinity *in vitro* and we have proposed that an analogous mutation in another
311 essential meiotic HORMAD, HTP-3^{H96Y}, behaves similarly (Russo et al., 2023). These mutations
312 suppress different meiotic defects in *pch-2* mutants *in vivo*, indicating that PCH-2 regulates pairing and
313 synapsis through its regulation of HTP-3 and crossover recombination through its regulation of HIM-3
314 (Russo et al., 2023). To determine which meiotic HORMAD PCH-2 might be regulating to affect
315 GFP::MSH-5's loading and removal on meiotic chromosomes, and the potential role for these early
316 crossover-eligible intermediates, we constructed *gfp::msh-5;htp-3^{H96Y}, gfp::msh-5;pch-2;htp-3^{H96Y},*
317 *gfp::msh-5;him-3^{R93Y}* and *gfp::msh-5;pch-2;him-3^{R93Y}* mutants and quantified GFP::MSH-5 foci
318 throughout the germline. Both *htp-3^{H96Y}* and *him-3^{R93Y}* mutants showed a drastic increase in the
319 average number of GFP::MSH-5 per row of nuclei throughout the germline (Figures 4C and 4D,
320 Supplemental Figure 1). For example, compared to control germlines that peaked at approximately an
321 average of 20 MSH-5 foci per row in early pachytene and then decreased in mid-pachytene, *him-3^{R93Y}*
322 germlines had closer to an average of 30 GFP::MSH-5 foci per row in early pachytene. Moreover, the
323 average number of GFP::MSH-5 foci per row increased further in mid and late pachytene, achieving
324 peaks closer to an average of 35 foci (Figure 4D). These very high numbers of GFP::MSH-5 were
325 striking but do not produce an increased number of crossovers in *htp-3^{H96Y}* or *him-3^{R93Y}* single mutants
326 (Russo et al., 2023), raising the possibility that not all of them reflect functional, crossover-specific
327 intermediates, similar to what has been observed in the absence of synapsis (Woglar and Villeneuve,

328 2018). These data also suggest that these mutations affect the behavior of GFP::MSH-5 on meiotic
329 chromosomes.

330

331 Quantification of GFP::MSH-5 foci in *pch-2;htp-3*^{H93Y} double mutants was similar to *htp-3*^{H93Y} single
332 mutants, suggesting that PCH-2's effect on the behavior of GFP::MSH-5 foci was not through its
333 regulation of HTP-3 (Supplemental Figure 1). In stark contrast to *pch-2;htp-3*^{H93Y} double mutants, the
334 *pch-2*;*him-3*^{R93Y} double mutant showed a dramatic decrease in the overall average of MSH-5 foci per
335 row throughout the germline (Figures 4C and 4D). These averages fell between the averages in
336 control and *pch-2* mutant animals, particularly in the transition zone and late pachytene (Figure 4D),
337 consistent with our previous report that this double mutant has fewer defects in crossover formation
338 than either single mutant (Russo et al., 2023). These data indicate that PCH-2's effect on promoting
339 the removal of GFP::MSH-5 in both the transition zone and mid to late pachytene is through its
340 regulation of HIM-3.

341

342 *pch-2* single mutants exhibit a loss of crossover assurance, as visualized by GFP::COSA-1 foci
343 (Figure 2B and Deshong et al., 2014). However, our quantification of GFP::MSH-5 in *pch-2* single
344 mutants in mid to late pachytene showed an increased number of crossover-eligible intermediates
345 (Figures 4A and 4B), suggesting a complex relationship between having too many crossover-eligible
346 intermediates and crossover assurance in *C. elegans*. To address this inconsistency, we generated
347 wildtype animals and *pch-2* mutants with both GFP::MSH-5 and a version of COSA-1 that has been
348 endogenously tagged at the N-terminus with the epitope tag, OLLAS (Janisiw et al., 2018), a fusion of
349 the *E. coli* OmpF protein and the mouse Langerin extracellular domain. Consistent with our and
350 others' previous findings, we observe a gradual reduction in the average number of GFP::MSH-5 foci
351 per row of nuclei in control animals as these nuclei approach the end of pachytene, ultimately
352 converging with the average number of OLLAS::COSA-1 foci per row (Figures 4E and 4F; Janisiw et
353 al., 2018; Woglar and Villeneuve, 2018). In addition, we consistently observed co-localization of

354 GFP::MSH-5 and OLLAS::COSA-1 foci in control animals, with a few MSH-5 foci persisting without
355 COSA-1, consistent with crossover designation (Figures 4E and 4F).

356

357 By contrast, we detected higher average numbers of GFP::MSH-5 foci per row across all late
358 pachytene nuclei in *pch-2* mutants and this average never converged upon the average number of
359 OLLAS::COSA-1 foci per row (Figures 4E and 4F). To test whether there was a correlation between
360 the number of GFP::MSH-5 foci and the loss of crossover assurance in *pch-2* mutants, we determined
361 the average number of GFP::MSH-5 foci in meiotic nuclei with 6 OLLAS::COSA-1 foci and those with
362 less than 6 OLLAS::COSA-1 foci in both control and *pch-2* mutant animals (Figures 4E and 4G,
363 Supplemental Figure 2). Indeed, we observed that *pch-2* mutant nuclei with less than 6
364 OLLAS::COSA-1 foci had significantly higher numbers of GFP::MSH-5 foci, compared to both control
365 and *pch-2* mutant nuclei with 6 OLLAS::COSA-1 foci (Figures 4E and 4G), suggesting that the inability
366 to reduce the number of crossover-eligible intermediates in *pch-2* mutants, counterintuitively, prevents
367 designation on some chromosomes and contributes to the observed loss of crossover assurance.

368

369 **PCH-2 is removed from the synaptonemal complex when crossovers are designated**

370

371 We have previously shown that PCH-2 localization to the SC is extended when there are partial
372 defects in synapsis or changes in karyotype, producing an increase in crossovers and a loss of
373 crossover interference (Deshong et al., 2014; Patel et al., 2023). These data led us to hypothesize that
374 PCH-2's presence on chromosomes promotes crossover formation. However, our quantification of
375 GFP::MSH-5 indicates that PCH-2 is required to limit the number of crossover-eligible intermediates,
376 in direct contrast to our proposed hypothesis (Figure 4). Therefore, we decided to revisit what role
377 PCH-2 localization to the SC might play in regulating crossover formation. To this end, we localized
378 PCH-2 in *dsb-2* mutants, in which DSB formation is substantially reduced and fewer crossovers are
379 formed in *C. elegans* (Rosu et al., 2013). We performed this experiment because, in budding yeast,

380 similar mutants that reduce DSB formation rely on Pch2 to successfully complete meiosis (Joshi et al.,
381 2009; Zanders and Alani, 2009).

382

383 Because the recombination defect in *dsb-2* mutants worsens with age (Rosu et al., 2013), we looked
384 at PCH-2 localization in both young (24 hours post L4 larval stage) and older animals (48 hours post
385 L4). We observed a unique and striking localization pattern in *dsb-2* mutants that we had not observed
386 before. When stained for PCH-2 and GFP::COSA-1, nuclei retain PCH-2 onto chromosomes far into
387 late pachytene, past the normal region when PCH-2 typically is removed from chromosomes (Figures
388 5A and 5B). However, unlike what we have observed in other mutants that have defects in synapsis or
389 changes in karyotype (Deshong et al., 2014; Patel et al., 2023), this retention of PCH-2 is not uniform
390 among all late pachytene nuclei in *dsb-2* mutants. Instead, most nuclei lose PCH-2 localization in late
391 pachytene while some retain it. We tested whether there was a relationship between the retention of
392 PCH-2 and the number of GFP::COSA-1 foci and found that 96% of nuclei that lose PCH-2 have at
393 least 1 GFP::COSA-1 focus (Figures 5A and 5B). In older animals (see 48 hours post-L4), this pattern
394 was even more clear: 77% of nuclei without PCH-2 had 1 or more GFP::COSA-1 focus and 93% of
395 meiotic nuclei without a GFP::COSA-1 focus retained PCH-2.

396

397 These data indicate that PCH-2's removal from the SC is in response to, coincident with or facilitates
398 crossover designation. To distinguish between these possibilities, we analyzed GFP::COSA-1 foci in
399 *dsb-2::AID* (Zhang et al., 2018) and *dsb-2::AID;pch-2* worms, reasoning that if PCH-2's removal is in
400 response to or coincident with designation, we should not detect any differences in the number of
401 GFP::COSA-1 foci in *dsb-2::AID* and *dsb-2::AID;pch-2* worms. We performed these experiments with
402 the auxin-inducible degradation system because of variability in the *dsb-2* mutant background that
403 affected reproducibility of our experiments.

404

405 Upon auxin treatment of *dsb-2::AID* worms, we observed a statistically significant (p value < 0.0001,
406 Mann-Whitney U test) decrease in the number of GFP::COSA-1 foci, in comparison with ethanol-
407 treated worms, verifying that we can reliably knock down DSB-2 with the AID system (Figure 5D).
408 When we performed the same experiment in *dsb-2::AID;pch-2* worms, the average number of
409 GFP::COSA-1 foci further decreased, indicating that fewer crossovers are designated when DSBs are
410 reduced and PCH-2 is absent (Figures 5C and 5D). These data argue against the possibility that PCH-
411 2's removal from the SC is simply in response to or coincident with crossover designation and instead,
412 suggest that PCH-2's removal from the SC somehow facilitates crossover designation and assurance.
413 Given the correlation between elevated GFP::MSH-5 foci and the loss of crossover assurance we
414 observe in *pch-2* mutants, we propose that PCH-2 is retained on meiotic chromosomes to ensure that
415 extra crossover-eligible intermediates are removed and crossover designation is delayed until
416 crossover assurance can be guaranteed in *C. elegans*.
417
418 **PCH-2 and high CHK-2 activity control the fate of early double strand breaks**
419
420 In *C. elegans*, meiotic cell cycle entry and progression depends on the activity of CHK-2, the meiosis-
421 specific ortholog of the DNA-damage kinase Chk2/CHEK2 (Baudrimont et al., 2022; Castellano-Pozo
422 et al., 2020; Kim et al., 2015; MacQueen and Villeneuve, 2001; Zhang et al., 2023) . Meiotic nuclei in
423 leptotene/zygotene are characterized by high CHK-2 activity, which drops to intermediate activity in
424 mid-pachytene (Kim et al., 2015; Zhang et al., 2023). In late pachytene, CHK-2 activity is inactivated
425 by the recruitment of polo-like kinase, PLK-2, to the SC, which enables crossover designation (Zhang
426 et al., 2023). Thus, CHK-2 activity also has consequences for the progression of meiotic
427 recombination and DNA repair.
428
429 Given that early DSBs are prevented from becoming crossovers by PCH-2 in early meiotic prophase,
430 we wanted to test if high CHK-2 activity in leptotene/zygotene also contributed to the fate of these
431 early DSBs. To evaluate this possibility, we used *syp-1*^{T452A} mutants (Sato-Carlton et al., 2018). The

432 SC component, SYP-1, is phosphorylated by cell cycle kinase, CDK-1, on T452, producing a Polo box
433 binding motif that recruits the polo-like kinase, PLK-2, to the SC, contributing to the inactivation of
434 CHK-2 when chromosomes are synapsed (Brandt et al., 2020; Zhang et al., 2023). Therefore, in *syp-*
435 *1*^{T452A} mutants, CHK-2 activity remains high throughout most of meiotic prophase in the *C. elegans*
436 germline, delaying meiotic progression as visualized by the extension of the transition zone (Figure
437 6A, Supplemental Figure 3).

438

439 We quantified the total number of GFP::COSA-1 foci in late pachytene nuclei in *syp-1*^{T452A} mutants
440 and observed a significant decrease in the average number of GFP::COSA-1 foci when compared to
441 control animals (Figures 6B and 6C), consistent with previous findings that *syp-1*^{T452A} mutants delay
442 designation and have fewer crossovers (Zhang et al., 2023). These data are also consistent with the
443 possibility that some DSBs fail to become crossovers when CHK-2 activity remains high. If this
444 hypothesis is correct, we predict that the combination of high CHK-2 activity and loss of *pch-2* should
445 produce more crossovers. We generated *pch-2;syp-1*^{T452A} double mutants to test this hypothesis.
446 These double mutants exhibited the same delay in meiotic progression as *syp-1*^{T452A} single mutants
447 (Supplemental Figure 3). When we quantified GFP::COSA-1 in *pch-2;syp-1*^{T452A} double mutants, we
448 detected a significant increase in the average number of GFP::COSA-1 foci compared to *syp-1*^{T452A}
449 single mutants (Figure 6C), in strong support of our hypothesis.

450

451 To further verify that the *pch-2* mutation suppresses the crossover defect in *syp-1*^{T452A} mutants, we
452 also monitored bivalent formation in diakinesis nuclei. *syp-1*^{T452A} single mutants exhibit an average of
453 7.12 DAPI staining bodies in diakinesis, higher than both control animals and *pch-2* single mutants
454 (Figure 6D). By contrast, *pch-2;syp-1*^{T452A} mutants had an average of 6.05 DAPI staining bodies
455 (Figure 6D and 6E), directly supporting our COSA-1 analysis and indicating that both PCH-2 function
456 and high CHK-2 activity collaborate to control the fate of DSBs and prevent some of them from
457 becoming crossovers in early meiotic prophase.

458

459 **Discussion**

460

461 We have shown that PCH-2 antagonizes crossover formation throughout meiotic prophase (Figures 2,
462 3, and 4) and that this regulation occurs through one of the three essential meiotic HORMADs in *C.*
463 *elegans*, HIM-3 (Figure 4). We propose that PCH-2 remodels HIM-3 on meiotic chromosomes to
464 destabilize crossover-eligible intermediates, visualized in our experiments as GFP-MSH-5 foci, thus
465 limiting which DSBs will become crossovers (Figure 7). However, this antagonism has different
466 consequences depending on when during meiotic prophase it occurs, underscoring the importance of
467 temporal regulation of these events. During leptotene/zygotene, when CHK-2 activity is high (Kim et
468 al., 2015; Zhang et al., 2023) and PCH-2 is present as foci on chromosomes (Deshong et al., 2014),
469 PCH-2 prevents crossover formation at some sites of initial DSB formation and early homolog
470 interactions (Figure 7B). In this way, PCH-2 promotes a wider distribution of crossovers across the
471 genome (Figure 1). In pachytene, when CHK-2 activity has decreased (Kim et al., 2015; Zhang et al.,
472 2023) and PCH-2 is localized to the SC (Deshong et al., 2014), PCH-2 winnows crossover-eligible
473 intermediates marked by GFP-MSH-5, ensuring their designation, colocalization with COSA-1 and
474 crossover assurance (Figure 7B). When there are defects in recombination, such as partial synapsis
475 (Deshong et al., 2014), changes in karyotype (Patel et al., 2023) or too few DSBs (Figure 5), PCH-2
476 persists on the SC to prevent designation, guarantee crossover assurance and some degree of
477 homeostasis, independent of an additional feedback mechanism that increases DSB formation (Patel
478 et al., 2023). That persistence of PCH-2 also disrupts crossover interference in two of these situations
479 (Deshong et al., 2014; Patel et al., 2023) strongly suggests that crossover interference is
480 mechanistically linked to assurance and homeostasis. For example, PCH-2's persistence on the
481 synaptonemal complex may maintain an extended period of competency for interhomolog repair, as
482 has been observed in mutants defective in crossover recombination (Rosu et al., 2011).

483

484 *him-3^{R93Y};pch-2* double mutants have stronger crossover assurance than either single mutant but less
485 than wildtype animals (Russo et al., 2023), a phenotype which can now be explained by the behavior
486 of GFP::MSH-5 foci in these double mutants (Figures 4C and 4D). We have shown that HIM-3^{R93Y}
487 mutant protein can adopt the closed conformation and loads on meiotic chromosomes similar to
488 wildtype HIM-3 (Russo et al., 2023). In vitro analysis shows that HIM-3^{R93Y} binds its closure motif with
489 reduced affinity, likely affecting its ability to adopt the closed conformation in vivo (Figure 7A and
490 Russo et al., 2023). The proposed role of PCH-2 in meiosis is to remodel meiotic HORMADs from the
491 closed conformation to the extended one (Figure 7A), regulating their association with chromosomes
492 (Bhalla, 2023). However, since meiotic HORMADs are not visibly depleted from chromosomes during
493 meiotic progression in *C. elegans* (Couteau et al., 2004; Couteau and Zetka, 2005; Goodyer et al.,
494 2008; Martinez-Perez and Villeneuve, 2005), this genetic interaction supports a role for PCH-2 in
495 temporarily reducing the occupancy of meiotic HORMADs on meiotic chromosomes, destabilizing
496 interactions with partner proteins that modulate the progression and fidelity of meiotic recombination
497 (Russo et al., 2023). Thus, PCH-2's remodeling of HIM-3 would disrupt protein-protein interactions
498 that underlie crossover-eligible intermediates, destabilizing them and reducing their number on
499 chromosomes, contributing to crossover control (Figure 7B). Since meiotic HORMADs are essential
500 for meiotic chromosome axis structure and function, our data therefore support a role for the meiotic
501 axis in crossover control, as suggested by previous reports (Chu et al., 2024; Girard et al., 2023;
502 Lambing et al., 2020; Nabeshima et al., 2004). However, the disassembly of crossover-eligible
503 intermediates would also release pro-crossover factors present at these sites, such as MSH-5, to
504 concentrate at other, more stable sites on the SC, facilitating designation during synapsis (Girard et
505 al., 2023; Yokoo et al., 2012). In this way, PCH-2's mechanism of action may reconcile current
506 competing models of crossover control (Girard et al., 2023). Moreover, these results raise the
507 possibility that this behavior of PCH-2 and/or meiotic HORMADs might be regulated by post-
508 translational modifications associated with crossover control, such as ubiquitination, SUMOylation and
509 phosphorylation (Gray and Cohen, 2016).

510

511 Given that mutation of PCH-2 produces changes in the number and distribution of crossovers across
512 multiple model systems, we argue that controlling crossover distribution and number is the conserved
513 role of PCH-2 in meiosis (Bhalla, 2023). We have previously proposed that the conserved role of PCH-
514 2 is to coordinate meiotic recombination with synapsis (Bhalla, 2023). With these results, we further
515 refine this model. Early in meiotic prophase, PCH-2 remodels meiotic HORMADs to prevent some
516 DSBs from becoming crossover-eligible intermediates, widening the recombination landscape beyond
517 early homolog interactions and/or sites that tend to be more favorable for DSB formation, also known
518 as “hot spots.” For example, this may explain the localization of TRIP13, the PCH-2 ortholog in mice,
519 to telomeres (Chotiner et al., 2024), sites that experience early homolog interactions due to the
520 organization of meiotic chromosomes in the bouquet formation (Scherthan et al., 1996). This
521 antagonism may also expand the regions of the genome that initiate synapsis in organisms that use
522 DSBs to accomplish this event. This possibility is supported by the observation that loss of TRIP13 in
523 mammals produce meiotic chromosomes that exhibit partial asynapsis (Roig et al., 2010), particularly
524 near regions that may act as barriers to SC polymerization (Brown et al., 2005; Roig et al., 2010).
525 Limiting which DSBs becomes crossover-eligible intermediates in early meiotic prophase also ensures
526 that meiotic recombination overlaps with synapsis, either completely, as in *C. elegans* (Yokoo et al.,
527 2012) or partially, as in budding yeast, plants and mice (Capilla-Perez et al., 2021; Cole et al., 2012;
528 Joshi et al., 2015; Morgan et al., 2021). Once synapsis is complete, PCH-2 continues to remodel
529 meiotic HORMADs on chromosomes to control the gradual implementation of crossover number and
530 distribution, reinforcing the important role that synapsis plays in mediating crossover control (Durand
531 et al., 2022; Libuda et al., 2013).
532
533 Unexpectedly, the inability to reduce the number of crossover-eligible intermediates in *pch-2* mutants,
534 as visualized by GFP::MSH-5 foci, does not produce extra crossovers but a loss of crossover-
535 assurance in *C. elegans* (Figure 4), a somewhat counterintuitive result. One interpretation of these
536 data is that crossover-eligible intermediates may be more numerous but absent from some
537 chromosomes in *pch-2* mutants, explaining the loss of crossover assurance. Since the absence of

538 crossover intermediates in *C. elegans* is accompanied by premature desynapsis of individual
539 chromosomes (Machovina et al., 2016; Pattabiraman et al., 2017) and chromosomes in *pch-2* mutants
540 delay desynapsis (Deshong et al., 2014), we do not favor this interpretation. Instead, we propose that
541 having too many crossover-eligible intermediates can be as deleterious to crossover assurance as
542 having too few (Figure 7B). This possibility is further supported by the loss of crossover assurance we
543 detect in irradiated wildtype worms, which is exacerbated in *pch-2* mutants (Figure 2).

544

545 This phenomenon, where crossover-eligible intermediates need to be winnowed to some threshold
546 number to ensure crossover assurance, may explain the loss of crossover assurance also observed in
547 *Trip13* deficient mice (Roig et al., 2010) and on small chromosomes in budding yeast (Chakraborty et
548 al., 2017). Alternatively, the counterintuitive relationship between the number of crossover-eligible
549 precursors and crossover assurance in *pch-2* mutants we observe might reflect an additional layer of
550 regulation during crossover formation specific to *C. elegans*. Since *C. elegans* chromosomes are
551 holocentric, crossovers play an additional role organizing chromosomes for the ordered release of
552 sister chromatid cohesion during meiosis I (Martinez-Perez et al., 2008; Nabeshima et al., 2005) and
553 extra crossovers can be deleterious to accurate chromosome segregation (Hollis et al., 2020). By
554 contrast, in *Arabidopsis*, a system that appears to be able to tolerate an extraordinarily high number of
555 crossovers with little to no effect on chromosome segregation (Durand et al., 2022), PCH2's inability to
556 localize to the SC produces an increase in crossover formation (Figure 7), as visualized by both MLH1
557 foci and the formation of chiasmata (Yang et al., 2022). Once again, an overarching theme that
558 becomes apparent in our model is that PCH-2 may play a common role in different systems, with
559 dramatic variations in phenotypic consequences given species-specific requirements and constraints.

560

561 We were not surprised to see high numbers of double crossovers on almost every chromosome in our
562 genetic analysis of recombination in wildtype worms, given our previous analysis (Deshong et al.,
563 2014). However, we were surprised to see that the majority of them were found near Pairing Centers

564 and sites of synapsis initiation, suggesting a relationship between early homolog interactions and the
565 formation of double crossovers. When we revisited our previous data, we observed similar patterns. In
566 addition, we do not detect these double crossovers cytologically in *C. elegans*, even when using the
567 OLLAS::COSA-1 reporter, which has been reported to identify double crossovers in spermatogenesis
568 not visualized by GFP::COSA-1 (Cahoon et al., 2023). Crossovers that are cytologically marked by
569 COSA-1 are known as Class I crossovers, which depend on pro-crossover factors such as MSH-5 and
570 ZHP-3, rely on synapsis and exhibit crossover control (Gray and Cohen, 2016). These data raise the
571 intriguing possibility that these double crossovers are the product of the alternate, Class II, pathway of
572 crossover formation, which relies on a different suite of proteins, does not respond to crossover
573 control, do not depend on synapsis and contributes to varying degrees in different model systems
574 (Gray and Cohen, 2016; Youds et al., 2010). Thus, based on the close, functional relationship that
575 exists between Class I crossovers and synapsis and the apparent antagonistic relationship that exists
576 between Class II crossovers and synapsis, important corollaries of our model may be that PCH-2
577 specifically coordinates recombination with synapsis to promote Class I crossovers, limit Class II
578 crossovers and that Class II crossovers are more likely to form early in meiosis, prior to synapsis.
579 Therefore, variations in the contribution of the Class II crossover pathways to crossover recombination
580 and the degree of cross-talk between Class I and Class II pathways among model systems might
581 reflect the degree to which crossover formation overlaps with synapsis (Bhalla, 2023; Gray and
582 Cohen, 2016; Yokoo et al., 2012). Furthermore, these corollaries are entirely consistent with PCH-2's
583 absence from the genome of fission yeast and Tetrahymena (Kops et al., 2020; Wu and Burgess,
584 2006), both systems in which chromosomes do not undergo meiotic synapsis, crossovers do not
585 exhibit interference and all crossovers are dependent on the Class II pathway (Hollingsworth and Brill,
586 2004; Lukaszewicz et al., 2013; Wolfe et al., 1976). However, this aspect of the model needs to be
587 formally tested.

588

589 Our results also have some additional important implications about the regulation of DSB formation
590 across the genome in *C. elegans*. It is formally possible that PCH-2 controls DSB distribution.

However, the complexity of recombination defects in *pch-2* mutants argues against this possibility. Instead, we explain the shift in the recombination landscape away from the central regions of chromosomes and toward PC ends in *pch-2* mutants (Figure 1) as a result of early DSBs becoming crossovers at the expense of later DSBs. This explanation is better supported by the panel of defects observed in *pch-2* mutants: DSBs introduced early in meiosis become crossover eligible intermediates and crossovers (Figures 2, 3 and 4) and while the number of DSBs are constant, DNA repair is accelerated (Deshong et al., 2014)**.** Moreover, this explanation suggests that when DSBs happen in meiotic prophase affects where they happen in the genome. Specifically, we propose that chromosome arms, which are gene poor, receive DSBs early during (or even throughout) DSB formation and the center of chromosomes, which are gene rich, receive DSBs later. The shift in recombination to the center of chromosomes when defects in meiosis prolong DSB formation provide further support to this possibility (Carlton et al., 2006; Deshong et al., 2014). A similar regulation of the timing of DSB formation has been demonstrated in budding yeast, where the DSB landscape across the whole genome expands when time in prophase is increased (Lopez Ruiz et al., 2024) and small, highly recombinogenic, chromosomes, get more DSBs later in meiotic prophase (Murakami et al., 2020; Subramanian et al., 2019). However, this temporal regulation has not been reported previously in *C. elegans* and suggests that this phenomenon is more widely conserved. This expansion of the DSB landscape in *C. elegans* to include the center regions of chromosomes later in meiosis may be a deliberate attempt for recombination to create new haplotypes for evolution to act on, despite the relative paucity of DSBs and the observation that they can result in chromosome missegregation (Altendorfer et al., 2020).

Finally, our work raises some important questions about the functional role(s) of DSBs in meiosis, aside from their contributions to crossover formation. Hicks and colleagues were the first to report that early DSBs do not contribute to crossover formation in *C. elegans* (Hicks et al., 2022). Here we show that these early DSBs are prevented from becoming crossovers by both PCH-2 activity and cell cycle stage, specifically in leptotene/zygotene, when homologs are initiating pairing and synapsis. In

618 budding yeast, similar, early-occurring DSBs have been characterized as “scout DSBs” because of
619 their preference for repair from sister chromatids, versus homologous chromosomes, and their
620 proposed role in contributing to homolog pairing (Borde and de Massy, 2015; Joshi et al., 2015). The
621 homolog bias that these “scout DSBs” do display seems dependent on budding yeast *PCH2* (Joshi et
622 al., 2015) but interpreting this experiment is complicated by the fact that Pch2 is also required to make
623 the budding yeast meiotic HORMAD, Hop1, available for its loading onto meiotic chromosomes
624 (Herruzo et al., 2021).

625

626 In contrast to budding yeast, *C. elegans* does not rely on DSBs to promote homolog pairing and
627 initiate synapsis (Dernburg et al., 1998); in worms, *cis*-acting sites called Pairing Centers are essential
628 for homolog pairing and synapsis (MacQueen et al., 2005). There is certainly some support in the
629 literature for DSBs playing a role in supporting pairing and synapsis in *C. elegans* (Guo et al., 2022;
630 Mlynarczyk-Evans et al., 2013; Roelens et al., 2015). However, if these early DSBs were contributing
631 to pairing and synapsis, we would expect to see a genetic interaction between *htp-3*^{H96Y} and *pch-2*
632 mutations in the installation of GFP::MSH-5 in the transition zone; we previously reported that *htp-*
633 *3*^{H96Y} suppresses the acceleration of pairing and synapsis of *pch-2* mutants, particularly when Pairing
634 Center function is compromised (Russo et al., 2023). Instead, we favor the possibility that these early
635 DSBs are generated to amplify the signaling of DNA damage kinases to prime them for their role in
636 recombination, a role that has also been proposed for “scout” DSBs (Joshi et al., 2015). That ATM-1, a
637 conserved DNA damage kinase that is downstream of CHK-2 in *C. elegans*, relies on DSBs for full
638 activity, supports this proposed, conserved role (Yu et al., 2023).

639

640 Our work provides an important framework to finally understand the role of PCH-2 in controlling the
641 number and distribution of crossovers, a role that we argue is its conserved role. While specific details
642 may vary across systems, we propose that PCH-2 remodels meiotic HORMADs throughout meiotic
643 prophase to destabilize crossover-eligible precursors, coordinating meiotic recombination with

644 synapsis, contributing to the progressive implementation of meiotic recombination and guaranteeing
645 crossover assurance, interference and homeostasis.
646
647 **Methods and Materials**
648
649 ***C.elegans* Genetics and Genome Engineering**
650 The *C. elegans* Bristol N2 was used as the wild-type strain. All strains were maintained at 20ºC under
651 standard conditions unless stated. Mutant combinations were generated by crossing. The following
652 mutants and rearrangements were used:
653
654 *LGII: pch-2(tm1458), meIs8 ([pie-1p::GFP::cosa-1 + unc-119(+)], dsb-2(me96), dsb-2(ie58[dsb-*
655 *2::AID::3xFLAG])*
656
657 *LGIII: cosa-1(ddr12[OLLAS::cosa-1]); htp-3(vc75)*
658
659 *LGIV: him-3(blt9), spo-11(ie59[spo-11::AID::3xFLAG]), msh-5[ddr22(GFP::msh-5)], ieSi38 [sun-*
660 *1p::TIR1::mRuby::sun-1 3'UTR + Cbr-unc-119(+)]*
661
662 *LGV: syp-1(icm85[T452A]), nT1[qIs51], bcIs39 (Plin-15::ced-1::GFP)*
663
664 **Genetic analysis of Recombination**
665 The wildtype Hawaiian CB4856 strain (HI) and the Bristol N2 strain were used to assay recombination
666 between single nucleotide polymorphisms (SNPs) on Chromosomes I, III, IV and X (Bazan and Hillers,
667 2011; Wicks et al., 2001). The SNPs, primers, enzymes used for restriction digests and expected
668 fragment sizes are included in Supplemental Table 1. To measure wild-type recombination, N2 males
669 containing *bcIs39* were crossed to Hawaiian CB4856 worms. Cross-progeny hermaphrodites were
670 identified by the presence of *bcIs39* and contained one N2 and one CB4856 chromosome. These

671 were assayed for recombination by crossing with CB4856 males containing *myo-2::mCherry*. Cross-
672 progeny hermaphrodites from the resulting cross were isolated as L4s, and then cultured individually
673 in 96- well plates in liquid S-media complete supplemented with HB101. Four days after initial
674 culturing, starved populations were lysed and used for PCR and restriction digest to detect N2 and
675 CB4856 SNP alleles.

676 For recombination in *pch-2* mutants, strains homozygous for the CB4856 background of the relevant
677 SNPs were created by backcrossing *pch-2* mutants to worms of the CB4856 background at least eight
678 times and verifying the presence of Hawaiian SNPs on all chromosomes tested in the recombination
679 assay. These Hawaiianized *pch-2* mutants were then mated with *pch-2; bcIs39*. Subsequent steps
680 were performed as in the wild-type worms.

681

682 **Immunostaining**

683 DAPI staining and immunostaining was performed as in (Russo et al., 2023), 20 to 24 hours post L4
684 unless otherwise noted. For analyzing bivalents, the same protocol was implemented with the
685 exception that hermaphrodites were dissected and DAPI stained 48 hours post late L4 stage, unless
686 otherwise noted.

687

688 The following primary antibodies were used at the indicated dilutions: alpaca anti-GFP Booster
689 (ChromoTek, gb2AF488) was used at 1:1000; rat anti-OLLAS (Invitrogen, PIMA516125) was used at
690 1:1000; and rabbit anti PCH-2 (Deshong et al., 2014) was used at 1:500. The following secondary
691 antibodies were used at the indicated dilutions: anti-rabbit Cy3 (Jackson Labs) was used at 1:500 and
692 anti-rat Cy5 (Jackson Labs) was used at 1:500

693

694 **Irradiation Experiments**

695 Control and *pch-2* mutant L4's were aged 12-14 hours before being exposed to 1,000 rad (10 Gy) of
696 X-ray radiation using a Precision MultiRad 160 X-irradiator (Precision X-Ray Inc.). Germlines were
697 then fixed and stained, 8 hours and 24 hours post irradiation.
698
699 **Auxin-induced Degradation Experiments**
700 Auxin treatment was performed by transferring young adult worms (aged 12-14 hours post-L4) to
701 bacteria-seeded plates containing auxin or 99% ethanol at specific time points, except for experiments
702 in which L4s were transferred directly to bacteria-seeded plates containing auxin or ethanol (the 36
703 hour and 48 hour time points in Figure 3C and E and the experiments in Figures 5C and D). The
704 natural auxin indole3-acetic acid (IAA) was purchased from Alfa Aesar (#A10556). A 400 mM stock
705 solution in ethanol was prepared and was stored at 4ºC for up to one month. Auxin was diluted to
706 100mM, and 100ul was spread onto NGM plates. Plates were allowed to dry before seeding with fresh
707 OP50 culture. Plates were left at 20ºC for 2-3 days in the dark to allow for bacterial lawn growth.
708
709 **Imaging and Quantification**
710 All images were acquired using a DeltaVision Personal DV system (Applied Precision) equipped with a
711 100X N.A. 1.40 oil-immersion objective (Olympus), resulting in an effective XY pixel spacing of 0.064
712 or 0.040 µm. Three-dimensional image stacks were collected at 0.2-µm Z spacing and processed by
713 constrained, iterative deconvolution. Image scaling, analysis and maximum-intensity projections were
714 performed using functions in the softWoRx software package.
715
716 For analysis of GFP::MSH-5 foci and meiotic progression, sum projections were generated using
717 ImageJ for each image of the germline. ImageJ plugins Cell Counter, ROI Manager, and Find Maxima
718 were used to identify and quantify GFP::MSH-5 foci by row from transition zone to the end of
719 pachytene. The threshold value was set depending on background conditions to ensure minimal
720 signals were identified. Foci were only quantified if they co-localized with DAPI staining. For all
721 genotypes, three germlines per genotype were analyzed and representative germlines are shown.

722

723 **Graphing and Statistical Analysis**

724 Data was analyzed using Python 3.8 and Prism for statistical significance. All datasets were tested for
725 normality using the Shapiro-Wilk test. For Figures 1, 2 and 5B, Fisher's exact test was used to
726 determine significance. For Figures 3, 4, 5D and 6, Mann-Whitney U test was used to determine
727 significance.

728

729 **Author contributions**

730 B.P., M.G., and N.B. designed the experiments. B.P., M.G., A.H., E.L., and V.O. performed the
731 experiments. B.P. and N.B. analyzed the data. B.P. and N.B. wrote the initial draft of the manuscript
732 and B.P., M.G., A.H. and N.B. revised the manuscript. N.B. acquired funding.

733

734 **Acknowledgements**

735 We would like to thank Josh Arribere, Pete Carlton, Abby Dernburg, Nicola Silva and Anne Villeneuve
736 for valuable strains and reagents. We would also like to thank the members of the Bhalla lab for
737 careful review of the manuscript. This work was supported by the NIH (grant numbers R35GM141835
738 [N.B.], R25GM051765 [V.O.] and T34GM140956 [A.H. and V.O.]). Some strains were provided by the
739 CGC, which is funded by NIH Office of Research Infrastructure Programs (P40 OD010440).

740

741 **References**

742 Altendorfer, E., L.I. Lascarez-Lagunas, S. Nadarajan, I. Mathieson, and M.P. Colaiacovo. 2020.
743 Crossover Position Drives Chromosome Remodeling for Accurate Meiotic Chromosome
744 Segregation. *Curr Biol*. 30:1329-1338 e1327.

745 Baudrimont, A., D. Paouneskou, A. Mohammad, R. Lichtenberger, J. Blundon, Y. Kim, M. Hartl, S.
746 Falk, T. Schedl, and V. Jantsch. 2022. Release of CHK-2 from PPM-1.D anchorage schedules
747 meiotic entry. *Sci Adv*. 8:eabl8861.

748 Bazan, G.C., and K.J. Hillers. 2011. SNP-based mapping of crossover recombination in
749 Caenorhabditis elegans. *Methods Mol Biol*. 745:207-222.

750 Bhalla, N. 2023. PCH-2 and meiotic HORMADs: A module for evolutionary innovation in meiosis? *Curr*
751 *Top Dev Biol*. 151:317-344.

752 Borde, V., and B. de Massy. 2015. Meiosis: early DNA double-strand breaks pave the way for inter-
753 homolog repair. *Dev Cell*. 32:663-664.

754 Borner, G.V., A. Barot, and N. Kleckner. 2008. Yeast Pch2 promotes domainal axis organization, timely
755 recombination progression, and arrest of defective recombinosomes during meiosis. *Proc Natl*
756 *Acad Sci U S A*. 105:3327-3332.

757 Brandt, J.N., K.A. Hussey, and Y. Kim. 2020. Spatial and temporal control of targeting Polo-like kinase
758 during meiotic prophase. *J Cell Biol*. 219.

759 Brown, P.W., L. Judis, E.R. Chan, S. Schwartz, A. Seftel, A. Thomas, and T.J. Hassold. 2005. Meiotic
760 synapsis proceeds from a limited number of subtelomeric sites in the human male. *Am J Hum*
761 *Genet*. 77:556-566.

762 Cahoon, C.K., C.J. Uebel, A.M. Villeneuve, and D.E. Libuda. 2023. Epitope tag-specific differences in
763 the detection of COSA-1 marked crossover sites in C. elegans spermatocytes. *MicroPubl Biol*.
764 2023.

765 Capilla-Perez, L., S. Durand, A. Hurel, Q. Lian, A. Chambon, C. Taochy, V. Solier, M. Grelon, and R.
766 Mercier. 2021. The synaptonemal complex imposes crossover interference and heterochiasmy
767 in Arabidopsis. *Proc Natl Acad Sci U S A*. 118.

768 Carlton, P.M., A.P. Farruggio, and A.F. Dernburg. 2006. A link between meiotic prophase progression
769 and crossover control. *PLoS Genet*. 2:e12.
770 Castellano-Pozo, M., S. Pacheco, G. Sioutas, A.L. Jaso-Tamame, M.H. Dore, M.M. Karimi, and E.
771 Martinez-Perez. 2020. Surveillance of cohesin-supported chromosome structure controls
772 meiotic progression. *Nat Commun*. 11:4345.
773 Chakraborty, P., A.V. Pankajam, G. Lin, A. Dutta, G.N. Krishnaprasad, M.M. Tekkedil, A. Shinohara,
774 L.M. Steinmetz, and K.T. Nishant. 2017. Modulating Crossover Frequency and Interference for
775 Obligate Crossovers in Saccharomyces cerevisiae Meiosis. *G3 (Bethesda)*. 7:1511-1524.
776 Chotiner, J.Y., N.A. Leu, F. Yang, I.G. Cossu, Y. Guan, H. Lin, and P.J. Wang. 2024. TRIP13 localizes
777 to synapsed chromosomes and functions as a dosage-sensitive regulator of meiosis. *Elife*. 12.
778 Chu, L., J. Zhuang, M. Geng, Y. Zhang, J. Zhu, C. Zhang, A. Schnittger, B. Yi, and C. Yang. 2024.
779 ASYNAPSIS3 has diverse dosage-dependent effects on meiotic crossover formation in
780 Brassica napus. *Plant Cell*. 36:3838-3856.
781 Cole, F., L. Kauppi, J. Lange, I. Roig, R. Wang, S. Keeney, and M. Jasin. 2012. Homeostatic control of
782 recombination is implemented progressively in mouse meiosis. *Nat Cell Biol*. 14:424-430.
783 Couteau, F., K. Nabeshima, A. Villeneuve, and M. Zetka. 2004. A component of C. elegans meiotic
784 chromosome axes at the interface of homolog alignment, synapsis, nuclear reorganization,
785 and recombination. *Curr Biol*. 14:585-592.
786 Couteau, F., and M. Zetka. 2005. HTP-1 coordinates synaptonemal complex assembly with homolog
787 alignment during meiosis in C. elegans. *Genes Dev*. 19:2744-2756.
788 Cuacos, M., C. Lambing, M. Pachon-Penalba, K. Osman, S.J. Armstrong, I.R. Henderson, E.
789 Sanchez-Moran, F.C.H. Franklin, and S. Heckmann. 2021. Meiotic chromosome axis
790 remodelling is critical for meiotic recombination in Brassica rapa. *J Exp Bot*. 72:3012-3027.
791 Dernburg, A.F., K. McDonald, G. Moulder, R. Barstead, M. Dresser, and A.M. Villeneuve. 1998. Meiotic
792 recombination in C. elegans initiates by a conserved mechanism and is dispensable for
793 homologous chromosome synapsis. *Cell*. 94:387-398.

794 Deshong, A.J., A.L. Ye, P. Lamelza, and N. Bhalla. 2014. A quality control mechanism coordinates
795 meiotic prophase events to promote crossover assurance. *PLoS Genet*. 10:e1004291.
796 Durand, S., Q. Lian, J. Jing, M. Ernst, M. Grelon, D. Zwicker, and R. Mercier. 2022. Joint control of
797 meiotic crossover patterning by the synaptonemal complex and HEI10 dosage. *Nat Commun*.
798 13:5999.
799 Girard, C., D. Zwicker, and R. Mercier. 2023. The regulation of meiotic crossover distribution: a coarse
800 solution to a century-old mystery? *Biochem Soc Trans*. 51:1179-1190.
801 Goodyer, W., S. Kaitna, F. Couteau, J.D. Ward, S.J. Boulton, and M. Zetka. 2008. HTP-3 links DSB
802 formation with homolog pairing and crossing over during C. elegans meiosis. *Dev Cell*. 14:263-
803 274.
804 Gray, S., and P.E. Cohen. 2016. Control of Meiotic Crossovers: From Double-Strand Break Formation
805 to Designation. *Annu Rev Genet*. 50:175-210.
806 Gu, Y., A. Desai, and K.D. Corbett. 2022. Evolutionary Dynamics and Molecular Mechanisms of
807 HORMA Domain Protein Signaling. *Annu Rev Biochem*. 91:541-569.
808 Guo, H., E.L. Stamper, A. Sato-Carlton, M.A. Shimazoe, X. Li, L. Zhang, L. Stevens, K.C.J. Tam, A.F.
809 Dernburg, and P.M. Carlton. 2022. Phosphoregulation of DSB-1 mediates control of meiotic
810 double-strand break activity. *Elife*. 11.
811 Hassold, T., and P. Hunt. 2001. To err (meiotically) is human: the genesis of human aneuploidy. *Nat*
812 *Rev Genet*. 2:280-291.
813 Haversat, J., A. Woglar, K. Klatt, C.C. Akerib, V. Roberts, S.Y. Chen, S. Arur, A.M. Villeneuve, and Y.
814 Kim. 2022. Robust designation of meiotic crossover sites by CDK-2 through phosphorylation of
815 the MutSgamma complex. *Proc Natl Acad Sci U S A*. 119:e2117865119.
816 Herruzo, E., A. Lago-Maciel, S. Baztan, B. Santos, J.A. Carballo, and P.A. San-Segundo. 2021. Pch2
817 orchestrates the meiotic recombination checkpoint from the cytoplasm. *PLoS Genet*.
818 17:e1009560.

819 Hicks, T., S. Trivedi, M. Eppert, R. Bowman, H. Tian, A. Dafalla, C. Crahan, S. Smolikove, and N.
820 Silva. 2022. Continuous double-strand break induction and their differential processing sustain
821 chiasma formation during Caenorhabditis elegans meiosis. *Cell Rep*. 40:111403.
822 Hollingsworth, N.M., and S.J. Brill. 2004. The Mus81 solution to resolution: generating meiotic
823 crossovers without Holliday junctions. *Genes Dev*. 18:117-125.
824 Hollis, J.A., M.L. Glover, A.J. Schlientz, C.K. Cahoon, B. Bowerman, S.M. Wignall, and D.E. Libuda.
825 2020. Excess crossovers impede faithful meiotic chromosome segregation in C. elegans.
826 *PLoS Genet*. 16:e1009001.
827 Janisiw, E., M.R. Dello Stritto, V. Jantsch, and N. Silva. 2018. BRCA1-BARD1 associate with the
828 synaptonemal complex and pro-crossover factors and influence RAD-51 dynamics during
829 Caenorhabditis elegans meiosis. *PLoS Genet*. 14:e1007653.
830 Jaramillo-Lambert, A., M. Ellefson, A.M. Villeneuve, and J. Engebrecht. 2007. Differential timing of S
831 phases, X chromosome replication, and meiotic prophase in the C. elegans germ line. *Dev*
832 *Biol*. 308:206-221.
833 Joshi, N., A. Barot, C. Jamison, and G.V. Borner. 2009. Pch2 links chromosome axis remodeling at
834 future crossover sites and crossover distribution during yeast meiosis. *PLoS Genet*.
835 5:e1000557.
836 Joshi, N., M.S. Brown, D.K. Bishop, and G.V. Borner. 2015. Gradual implementation of the meiotic
837 recombination program via checkpoint pathways controlled by global DSB levels. *Mol Cell*.
838 57:797-811.
839 Joyce, E.F., and K.S. McKim. 2009. Drosophila PCH2 is required for a pachytene checkpoint that
840 monitors double-strand-break-independent events leading to meiotic crossover formation.
841 *Genetics*. 181:39-51.
842 Keeney, S., C.N. Giroux, and N. Kleckner. 1997. Meiosis-specific DNA double-strand breaks are
843 catalyzed by Spo11, a member of a widely conserved protein family. *Cell*. 88:375-384.

844 Kelly, K.O., A.F. Dernburg, G.M. Stanfield, and A.M. Villeneuve. 2000. Caenorhabditis elegans msh-5
845 is required for both normal and radiation-induced meiotic crossing over but not for completion
846 of meiosis. *Genetics*. 156:617-630.
847 Kim, Y., N. Kostow, and A.F. Dernburg. 2015. The Chromosome Axis Mediates Feedback Control of
848 CHK-2 to Ensure Crossover Formation in C. elegans. *Dev Cell*. 35:247-261.
849 Kim, Y., S.C. Rosenberg, C.L. Kugel, N. Kostow, O. Rog, V. Davydov, T.Y. Su, A.F. Dernburg, and K.D.
850 Corbett. 2014. The chromosome axis controls meiotic events through a hierarchical assembly
851 of HORMA domain proteins. *Dev Cell*. 31:487-502.
852 Kops, G., B. Snel, and E.C. Tromer. 2020. Evolutionary Dynamics of the Spindle Assembly Checkpoint
853 in Eukaryotes. *Curr Biol*. 30:R589-R602.
854 Lambing, C., P.C. Kuo, A.J. Tock, S.D. Topp, and I.R. Henderson. 2020. ASY1 acts as a dosage-
855 dependent antagonist of telomere-led recombination and mediates crossover interference in
856 Arabidopsis. *Proc Natl Acad Sci U S A*. 117:13647-13658.
857 Lambing, C., K. Osman, K. Nuntasoontorn, A. West, J.D. Higgins, G.P. Copenhaver, J. Yang, S.J.
858 Armstrong, K. Mechtler, E. Roitinger, and F.C. Franklin. 2015. Arabidopsis PCH2 Mediates
859 Meiotic Chromosome Remodeling and Maturation of Crossovers. *PLoS Genet*. 11:e1005372.
860 Libuda, D.E., S. Uzawa, B.J. Meyer, and A.M. Villeneuve. 2013. Meiotic chromosome structures
861 constrain and respond to designation of crossover sites. *Nature*. 502:703-706.
862 Lopez Ruiz, L.M., D. Johnson, W.H. Gittens, G.G.B. Brown, R.M. Allison, and M.J. Neale. 2024.
863 Meiotic prophase length modulates Tel1-dependent DNA double-strand break interference.
864 *PLoS Genet*. 20:e1011140.
865 Lukaszewicz, A., R.A. Howard-Till, and J. Loidl. 2013. Mus81 nuclease and Sgs1 helicase are
866 essential for meiotic recombination in a protist lacking a synaptonemal complex. *Nucleic Acids*
867 *Res*. 41:9296-9309.
868 Machovina, T.S., R. Mainpal, A. Daryabeigi, O. McGovern, D. Paouneskou, S. Labella, M. Zetka, V.
869 Jantsch, and J.L. Yanowitz. 2016. A Surveillance System Ensures Crossover Formation in C.
870 elegans. *Curr Biol*. 26:2873-2884.

871 MacQueen, A.J., C.M. Phillips, N. Bhalla, P. Weiser, A.M. Villeneuve, and A.F. Dernburg. 2005.
872 Chromosome sites play dual roles to establish homologous synapsis during meiosis in C.
873 elegans. *Cell*. 123:1037-1050.
874 MacQueen, A.J., and A.M. Villeneuve. 2001. Nuclear reorganization and homologous chromosome
875 pairing during meiotic prophase require C. elegans chk-2. *Genes Dev*. 15:1674-1687.
876 Martinez-Perez, E., M. Schvarzstein, C. Barroso, J. Lightfoot, A.F. Dernburg, and A.M. Villeneuve.
877 2008. Crossovers trigger a remodeling of meiotic chromosome axis composition that is linked
878 to two-step loss of sister chromatid cohesion. *Genes Dev*. 22:2886-2901.
879 Martinez-Perez, E., and A.M. Villeneuve. 2005. HTP-1-dependent constraints coordinate homolog
880 pairing and synapsis and promote chiasma formation during C. elegans meiosis. *Genes Dev*.
881 19:2727-2743.
882 Mlynarczyk-Evans, S., B. Roelens, and A.M. Villeneuve. 2013. Evidence that masking of synapsis
883 imperfections counterbalances quality control to promote efficient meiosis. *PLoS Genet*.
884 9:e1003963.
885 Morgan, C., J.A. Fozard, M. Hartley, I.R. Henderson, K. Bomblies, and M. Howard. 2021. Diffusion-
886 mediated HEI10 coarsening can explain meiotic crossover positioning in Arabidopsis. *Nat*
887 *Commun*. 12:4674.
888 Murakami, H., I. Lam, P.C. Huang, J. Song, M. van Overbeek, and S. Keeney. 2020. Multilayered
889 mechanisms ensure that short chromosomes recombine in meiosis. *Nature*. 582:124-128.
890 Nabeshima, K., A.M. Villeneuve, and M.P. Colaiacovo. 2005. Crossing over is coupled to late meiotic
891 prophase bivalent differentiation through asymmetric disassembly of the SC. *J Cell Biol*.
892 168:683-689.
893 Nabeshima, K., A.M. Villeneuve, and K.J. Hillers. 2004. Chromosome-wide regulation of meiotic
894 crossover formation in Caenorhabditis elegans requires properly assembled chromosome
895 axes. *Genetics*. 168:1275-1292.

896 Nadarajan, S., E. Altendorfer, T.T. Saito, M. Martinez-Garcia, and M.P. Colaiacovo. 2021. HIM-17
897 regulates the position of recombination events and GSP-1/2 localization to establish short arm
898 identity on bivalents in meiosis. *Proc Natl Acad Sci U S A*. 118.
899 Patel, B., M. Grobler, and N. Bhalla. 2023. Chromosomal fusions, but not chromosomal inversions,
900 activate a PCH-2 dependent checkpoint that promotes crossover formation in C. elegans.
901 *MicroPubl Biol*. 2023.
902 Pattabiraman, D., B. Roelens, A. Woglar, and A.M. Villeneuve. 2017. Meiotic recombination modulates
903 the structure and dynamics of the synaptonemal complex during C. elegans meiosis. *PLoS*
904 *Genet*. 13:e1006670.
905 Roelens, B., M. Schvarzstein, and A.M. Villeneuve. 2015. Manipulation of Karyotype in Caenorhabditis
906 elegans Reveals Multiple Inputs Driving Pairwise Chromosome Synapsis During Meiosis.
907 *Genetics*. 201:1363-1379.
908 Roig, I., J.A. Dowdle, A. Toth, D.G. de Rooij, M. Jasin, and S. Keeney. 2010. Mouse TRIP13/PCH2 is
909 required for recombination and normal higher-order chromosome structure during meiosis.
910 *PLoS Genet*. 6.
911 Rosu, S., D.E. Libuda, and A.M. Villeneuve. 2011. Robust crossover assurance and regulated
912 interhomolog access maintain meiotic crossover number. *Science*. 334:1286-1289.
913 Rosu, S., K.A. Zawadzki, E.L. Stamper, D.E. Libuda, A.L. Reese, A.F. Dernburg, and A.M. Villeneuve.
914 2013. The C. elegans DSB-2 protein reveals a regulatory network that controls competence for
915 meiotic DSB formation and promotes crossover assurance. *PLoS Genet*. 9:e1003674.
916 Russo, A.E., S. Giacopazzi, A. Deshong, M. Menon, V. Ortiz, K.M. Ego, K.D. Corbett, and N. Bhalla.
917 2023. The conserved AAA ATPase PCH-2 distributes its regulation of meiotic prophase events
918 through multiple meiotic HORMADs in C. elegans. *PLoS Genet*. 19:e1010708.
919 Sato-Carlton, A., C. Nakamura-Tabuchi, S.K. Chartrand, T. Uchino, and P.M. Carlton. 2018.
920 Phosphorylation of the synaptonemal complex protein SYP-1 promotes meiotic chromosome
921 segregation. *J Cell Biol*. 217:555-570.

922 Scherthan, H., S. Weich, H. Schwegler, C. Heyting, M. Harle, and T. Cremer. 1996. Centromere and
923 telomere movements during early meiotic prophase of mouse and man are associated with the
924 onset of chromosome pairing. *J Cell Biol*. 134:1109-1125.
925 Snowden, T., S. Acharya, C. Butz, M. Berardini, and R. Fishel. 2004. hMSH4-hMSH5 recognizes
926 Holliday Junctions and forms a meiosis-specific sliding clamp that embraces homologous
927 chromosomes. *Mol Cell*. 15:437-451.
928 Subramanian, V.V., X. Zhu, T.E. Markowitz, L.A. Vale-Silva, P.A. San-Segundo, N.M. Hollingsworth, S.
929 Keeney, and A. Hochwagen. 2019. Persistent DNA-break potential near telomeres increases
930 initiation of meiotic recombination on short chromosomes. *Nat Commun*. 10:970.
931 Veller, C., N. Kleckner, and M.A. Nowak. 2019. A rigorous measure of genome-wide genetic shuffling
932 that takes into account crossover positions and Mendel's second law. *Proc Natl Acad Sci U S*
933 *A*. 116:1659-1668.
934 Wicks, S.R., R.T. Yeh, W.R. Gish, R.H. Waterston, and R.H. Plasterk. 2001. Rapid gene mapping in
935 Caenorhabditis elegans using a high density polymorphism map. *Nat Genet*. 28:160-164.
936 Woglar, A., and A.M. Villeneuve. 2018. Dynamic Architecture of DNA Repair Complexes and the
937 Synaptonemal Complex at Sites of Meiotic Recombination. *Cell*. 173:1678-1691 e1616.
938 Wojtasz, L., K. Daniel, I. Roig, E. Bolcun-Filas, H. Xu, V. Boonsanay, C.R. Eckmann, H.J. Cooke, M.
939 Jasin, S. Keeney, M.J. McKay, and A. Toth. 2009. Mouse HORMAD1 and HORMAD2, two
940 conserved meiotic chromosomal proteins, are depleted from synapsed chromosome axes with
941 the help of TRIP13 AAA-ATPase. *PLoS Genet*. 5:e1000702.
942 Wolfe, J., B. Hunter, and W.S. Adair. 1976. A cytological study of micronuclear elongation during
943 conjugation in Tetrahymena. *Chromosoma*. 55:289-308.
944 Wu, H.Y., and S.M. Burgess. 2006. Two distinct surveillance mechanisms monitor meiotic
945 chromosome metabolism in budding yeast. *Curr Biol*. 16:2473-2479.
946 Yang, C., B. Hu, S.M. Portheine, P. Chuenban, and A. Schnittger. 2020. State changes of the HORMA
947 protein ASY1 are mediated by an interplay between its closure motif and PCH2. *Nucleic Acids*
948 *Res*. 48:11521-11535.

949 Yang, C., K. Sofroni, Y. Hamamura, B. Hu, H.T. Elbasi, M. Balboni, L. Chu, D. Stang, M. Heese, and A.
950 Schnittger. 2022. ZYP1-mediated recruitment of PCH2 to the synaptonemal complex remodels
951 the chromosome axis leading to crossover restriction. *Nucleic Acids Res*. 50:12924-12937.
952 Yokoo, R., K.A. Zawadzki, K. Nabeshima, M. Drake, S. Arur, and A.M. Villeneuve. 2012. COSA-1
953 reveals robust homeostasis and separable licensing and reinforcement steps governing
954 meiotic crossovers. *Cell*. 149:75-87.
955 Youds, J.L., D.G. Mets, M.J. McIlwraith, J.S. Martin, J.D. Ward, O.N. NJ, A.M. Rose, S.C. West, B.J.
956 Meyer, and S.J. Boulton. 2010. RTEL-1 enforces meiotic crossover interference and
957 homeostasis. *Science*. 327:1254-1258.
958 Yu, Z., H.J. Kim, and A.F. Dernburg. 2023. ATM signaling modulates cohesin behavior in meiotic
959 prophase and proliferating cells. *Nat Struct Mol Biol*. 30:436-450.
960 Yu, Z., Y. Kim, and A.F. Dernburg. 2016. Meiotic recombination and the crossover assurance
961 checkpoint in Caenorhabditis elegans. *Semin Cell Dev Biol*. 54:106-116.
962 Zanders, S., and E. Alani. 2009. The pch2Delta mutation in baker's yeast alters meiotic crossover
963 levels and confers a defect in crossover interference. *PLoS Genet*. 5:e1000571.
964 Zhang, L., W. Stauffer, D. Zwicker, and A.F. Dernburg. 2021. Crossover patterning through kinase-
965 regulated condensation and coarsening of recombination nodules. *bioRxiv*.
966 Zhang, L., W.T. Stauffer, J.S. Wang, F. Wu, Z. Yu, C. Liu, H.J. Kim, and A.F. Dernburg. 2023.
967 Recruitment of Polo-like kinase couples synapsis to meiotic progression via inactivation of
968 CHK-2. *Elife*. 12.
969

970 **Figure Legends**

971

972 **Figure 1. PCH-2 controls the number and distribution of crossovers in similar patterns on**
973 **multiple chromosomes.** Genetic analysis of meiotic recombination in wildtype and *pch-2* mutants.
974 DCO indicates double crossovers. Physical and genetic maps of Chromosome I, III, IV and the X
975 chromosome are depicted to scale. Genetic distance is shown in centimorgans. A * indicates a p-value
976 < 0.05, a ** indicates a p value < 0.01 and a *** indicates p-value < 0.001.

977

978

979 **Figure 2. PCH-2 prevents exogenous double strand breaks from becoming crossovers in early**
980 **meiotic prophase. A.** Illustration of the irradiation experiments in control and *pch-2* mutants. Box
981 indicates late pachytene, the area where GFP::COSA-1 foci are analyzed. **B.** Fraction of meiotic
982 nuclei with less than 6, 6, or greater than 6 GFP::COSA-1 foci in control animals (yellow, n = 446) and
983 *pch-2* mutants (blue, n = 552). **C.** Meiotic nuclei in control animals and *pch-2* mutants 8 hours post
984 irradiation stained for DAPI (magenta) and GFP::COSA-1 (green). Scale bar is 4 um. **D.** Fraction of
985 meiotic nuclei with less than 6, 6, or greater than 6 GFP::COSA-1 foci in control animals (yellow, n =
986 143) and *pch-2* mutants (blue, n = 125) 8 hours post irradiation. **E.** Meiotic nuclei in control animals
987 and *pch-2* mutants 24 hours post irradiation with DAPI (magenta) and GFP::COSA-1 (green). **F.**
988 Fraction of meiotic nuclei with less than 6, 6, or greater than 6 GFP::COSA-1 foci in control animals (n
989 = 179) and *pch-2* mutants (n = 378) 24 hours post irradiation. A *** indicates p-value < 0.001, and a
990 **** indicates p-value < 0.0001.

991

992 **Figure 3. PCH-2 prevents SPO-11-induced double strand breaks from becoming crossovers in**
993 **early meiotic prophase. A.** Illustration of the SPO-11 depletion experiment to assay GFP::COSA-1 in
994 control animals and *pch-2* mutants at different timepoints of auxin treatment. Each timepoint indicates
995 when SPO-11 is depleted in the germline with auxin induced degradation. Box indicates late
996 pachytene, the area where GFP::COSA-1 foci are analyzed. **B.** Representative images of meiotic

997 nuclei in control animals and *pch-2* mutants treated with auxin for 20 hours, stained for DAPI
998 (magenta) and GFP::COSA-1 (green). Scale bar is 5 um. **C.** Number of GFP::COSA-1 foci in meiotic
999 nuclei at different timepoints of auxin treatment in control (blue) and *pch-2* mutants (yellow). Error bars
1000 represent standard error of the mean (SEM). N values are as follows: 36 hours on auxin, control (78
1001 nuclei) and *pch-2* (83 nuclei); 24 hours on auxin, control (132 nuclei) and *pch-2* (155 nuclei); 22 hours
1002 on auxin, control (152 nuclei) and *pch-2* (168 nuclei); 20 hours on auxin, control (139 nuclei) and *pch-*
1003 *2* (157 nuclei); 18 hours on auxin, control (154 nuclei) and *pch-2* (154 nuclei); and 24 hours on
1004 ethanol, control (86 nuclei) and *pch-2* (143 nuclei). **D.** Illustration of the SPO-11 depletion experiment
1005 to assay bivalents in control animals and *pch-2* mutants at different timepoints of auxin treatment.
1006 Each timepoint indicates when SPO-11 is depleted in the germline with auxin induced degradation.
1007 Box indicates diakinesis, where DAPI stained bodies are analyzed. **E.** Oocytes from control animals
1008 and *pch-2* mutants stained for DAPI (magenta). Scale bar is 4um. **F**. Number of DAPI stained bodies
1009 in meiotic nuclei at different timepoints of auxin treatment in control animals and *pch-2* mutants. N
1010 values are as follows: 48 hours on auxin, control (47 nuclei) and *pch-2* (43 nuclei); 36 hours on auxin,
1011 control (46 nuclei) and *pch-2* (50 nuclei); 34 hours on auxin, control (41 nuclei) and *pch-2* (41 nuclei);
1012 32 hours on auxin, control (51 nuclei) and *pch-2* (47 nuclei); 30 hours on auxin, control (46 nuclei) and
1013 *pch-2* (21 nuclei); and 36 hours on ethanol, control (52 nuclei) and *pch-2* (48 nuclei). Error bars
1014 represent SEM and a * indicates p-value < 0.05 and a *** indicates p-value < 0.001.
1015
1016 **Figure 4. PCH-2 is required for timely loading and removal of MSH-5 on meiotic chromosomes**
1017 **through its regulation of HIM-3. A.** Representative images of nuclei in different stages of meiotic
1018 prophase in control animals and *pch-2* mutants stained for DAPI (magenta) and GFP::MSH-5 (green)
1019 Scale bar is 5 um. **B.** Scatter plot showing average GFP::MSH-5 foci per row of germline nuclei in
1020 control animals (yellow, 163 nuclei) and *pch-2* mutants (blue, 195 nuclei) from the transition zone (TZ)
1021 to late pachytene (LP), normalized to 100. The line represents a rolling average of four rows. **C.**
1022 Representative images of nuclei in different stages of meiotic prophase in *him-3*^{R93Y} mutants (left) and
1023 *pch-2*;*him-3*^{R93Y} double mutants (right), stained for DAPI (magenta) and GFP::MSH-5 (green). **D.**

1024 Scatter plot showing average GFP::MSH-5 foci per row in *him-3*^{R93Y} (brown, 183 nuclei) and *pch-*
1025 *2;him-3*^{R93Y} mutants (pink, 163 nuclei) from the transition zone (TZ) to late pachytene (LP), normalized
1026 to 100. The line represents a rolling average of four rows. Similar data is provided for a control
1027 germline (opaque yellow, 236 nuclei) for comparison. **E.** Representative images of meiotic nuclei in
1028 control animals and *pch-2* mutants stained for DAPI (blue), GFP::MSH-5 (green), and OLLAS::COSA-
1029 1 (red). Yellow circles indicate GFP::MSH-5 without OLLAS::COSA-1. Scale bar is 4um. **F.** Scatter plot
1030 showing average GFP::MSH-5 (green) and OLLAS::COSA-1 (red) foci per row in the last five rows of
1031 the germline in control animals (36 nuclei) and *pch-2* mutants (45 nuclei). The line represents a rolling
1032 average of 2 rows. **G.** Swarm plot showing number of GFP::MSH-5 foci in control (yellow, 14 nuclei)
1033 and *pch-2* mutant (blue, 29 nuclei) nuclei with less than 6 OLLAS::COSA-1 foci (left) and 6
1034 OLLAS::COSA-1 foci (right). Error bars represent SEM. A * indicates a p-value less than 0.05 and a **
1035 indicates a p-value < 0.01.

1036

1037 **Figure 5. PCH-2 is removed when crossovers are designated. A.** Representative images of
1038 meiotic nuclei in *dsb-2* animals 24 hours post L4 and 48 hours post L4 stained for DAPI (magenta),
1039 PCH-2 (red), and GFP::COSA-1 (green). Scale bar is 4 um. **B.** Stacked histograms showing
1040 percentage of PCH-2 positive (n = 43 at 24 hours, n = 42 at 48 hours) and negative (n = 194 at 24
1041 hours, n = 130 at 48 hours) nuclei with (lime) and without (dark green) GFP::COSA-1 foci in *dsb-2*
1042 mutants at 24 hours post L4 and 48 hours post L4. **C.** Representative images of meiotic nuclei in *dsb-*
1043 *2::AID* and *dsb-2::AID;pch-2* mutants treated with auxin and stained for DAPI (magenta) and
1044 GFP::COSA-1 (green). Scale bar is 5 um. **D.** Swarm plot showing the number of GFP::COSA-1 foci in
1045 *dsb-2::AID* (gray) and *dsb-2::AID;pch-2* (lemon) mutants when treated with ethanol or auxin. N values
1046 are as follows: *dsb-2::AID* (101 nuclei) and *dsb-2::AID;pch-2* (154 nuclei) on ethanol, *dsb-2::AID* (136
1047 nuclei) and *dsb-2::AID;pch-2* (131 nuclei) on auxin. Error bars represent the SEM. A ** indicates a p-
1048 value less than 0.01 and a **** indicates p-value < 0.0001.

1049

1050 **Figure 6. PCH-2 and high CHK-2 activity control the fate of early double strand breaks.** A.
1051 Illustration of CHK-2 activity in wildtype and *syp-1*^{T452A} germlines. **B.** Representative images of meiotic
1052 nuclei late pachytene in *syp-1*^{T452A} and *pch-2;syp-1*^{T452A} mutants stained for DAPI (magenta) and
1053 GFP::COSA-1 (green). Scale bar is 5 um. **C.** Swarm plot showing number of GFP::COSA-1 foci in
1054 control animals (blue), *pch-2* (yellow), *syp-1*^{T452A} (maroon), and *pch-2;syp-1*^{T452A} (light blue) mutants.
1055 Error bars represent SEM. **D.** Oocytes from *syp-1*^{T452A} and *pch-2;syp-1*^{T452A} mutant worms stained for
1056 DAPI (magenta). Scale bar is 4um. **D.** Swarm plot showing number of DAPI stained bodies in control
1057 animals (blue, n = 154), *pch-2* (yellow, n = 89), *syp-1*^{T452A} (maroon, n = 247)), and *pch-2;syp-1*^{T452A}
1058 (light blue, n = 242) mutants. Error bars represent SEM. A **** indicates p-value < 0.0001.
1059
1060 **Figure 7. PCH-2 remodels HIM-3 to disassemble crossover-eligible intermediates, controlling**
1061 **crossover distribution and number. A.** Model for how *pch-2* and *him-3*^{R93Y} mutations genetically
1062 interact to affect the progression of meiotic recombination. HIM-3 adopts the closed conformation
1063 upon binding an interacting protein with a closure motif and its conversion to the extended
1064 conformation is facilitated by PCH-2's remodeling of its HORMA domain. **B.** Model for how PCH-2 and
1065 HIM-3 progressively implement meiotic recombination during different stages of meiotic prophase.
1066
1067 **Supplemental Figure 1: PCH-2 does not regulate GFP::MSH-5 loading and removal through**
1068 **HTP-3. A.** Representative images of nuclei in different stages of meiotic prophase in *htp-3*^{H96Y} and
1069 *pch-2; htp-3*^{H96Y} mutants stained for DAPI (magenta) and GFP::MSH-5 (green) Scale bar in all images
1070 is 5 um. **B.** Scatter plot showing average GFP::MSH-5 foci per row of germline nuclei in *htp-3*^{H96Y}
1071 (blue, 132 nuclei) and *pch-2; htp-3*^{H96Y} (green, 161 nuclei) mutants from the transition zone to late
1072 pachytene, normalized to 100. The line represents a rolling average of four rows. Similar data is
1073 provided for a control germline (opaque yellow, 163 nuclei) for comparison
1074

1075 **Supplemental Figure 2: *pch-2* meiotic nuclei with elevated numbers of GFP::MSH-5 foci show**
1076 **defects in crossover assurance.** Gray scale images of control and *pch-2* mutant nuclei stained for
1077 DAPI, GFP::MSH-5 and OLLAS::COSA-1. Scale bar in image is 4 um.
1078
1079 **Supplemental Figure 3: *syp-1*^{T452A} and *pch-2;syp-1*^{T452A} mutants display a similar defect in**
1080 **meiotic progression. A.** Representative images of *syp-1*^{T452A} and *pch-2;syp-1*^{T452A} mutant germlines.
1081 Encircled nuclei indicate transition zone nuclei. Scale bar indicates 10 um. **B.** Quantification of fraction
1082 of rows of transition zone nuclei in 3 germlines in *syp-1*^{T452A} (maroon) and *pch-2;syp-1*^{T452A} (light blue)
1083 mutants.
1084
1085
1086

Figure 1

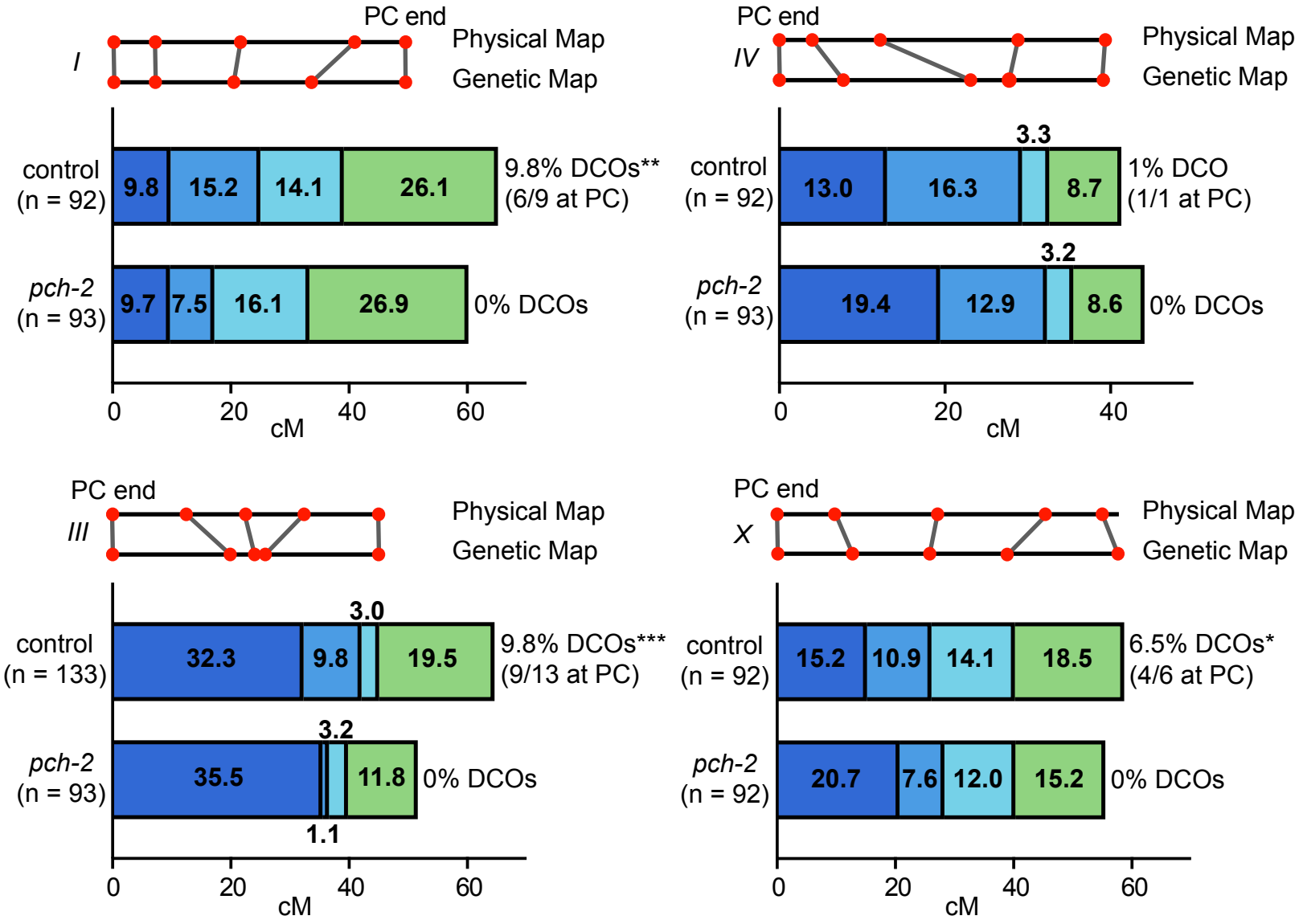
PC end
I
Physical Map
Genetic Map
control
(n = 92)
9.8
15.2
14.1
26.1
9.8% DCOs**
(6/9 at PC)
pch-2
(n = 93)
9.7
7.5
16.1
26.9
0% DCOs
0
20
40
60
cM
PC end
IV
Physical Map
Genetic Map
control
(n = 92)
13.0
16.3
3.3
8.7
1% DCO
(1/1 at PC)
pch-2
(n = 93)
19.4
12.9
3.2
8.6
0% DCOs
0
20
40
cM
PC end
III
Physical Map
Genetic Map
control
(n = 133)
32.3
9.8
3.0
19.5
9.8% DCOs***
(9/13 at PC)
pch-2
(n = 93)
35.5
1.1
3.2
11.8
0% DCOs
0
20
40
60
cM
PC end
X
Physical Map
Genetic Map
control
(n = 92)
15.2
10.9
14.1
18.5
6.5% DCOs*
(4/6 at PC)
pch-2
(n = 92)
20.7
7.6
12.0
15.2
0% DCOs
0
20
40
60
cM

A

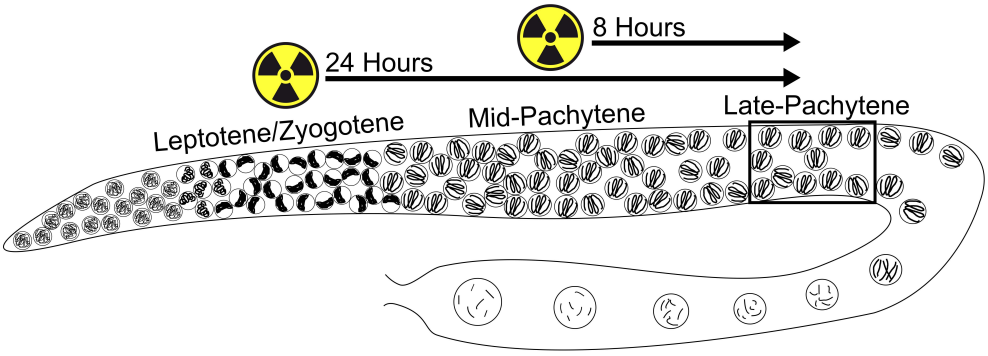
8 Hours
24 Hours
Leptotene/Zygotene
Mid-Pachytene
Late-Pachytene

B

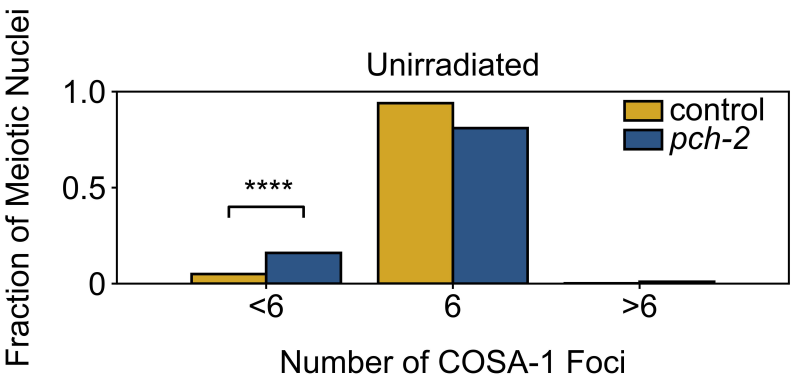
Unirradiated
Fraction of Meiotic Nuclei
1.0
0.5
0
control
pch-2
****
<6
6
>6
Number of COSA-1 Foci

C

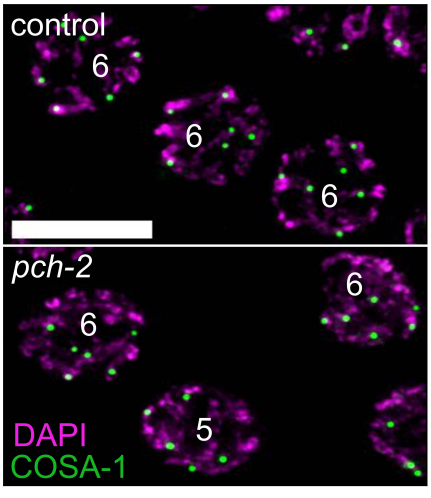
8 Hours Post Irradiation
control
6
6
6
pch-2
6
6
5
DAPI
COSA-1

D

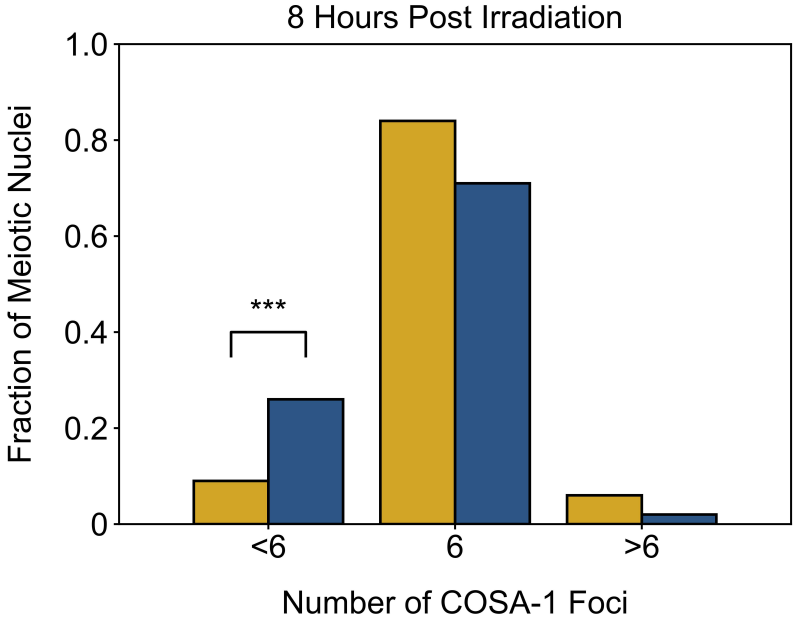
8 Hours Post Irradiation
Fraction of Meiotic Nuclei
1.0
0.8
0.6
0.4
0.2
0
***
<6
6
>6
Number of COSA-1 Foci

E

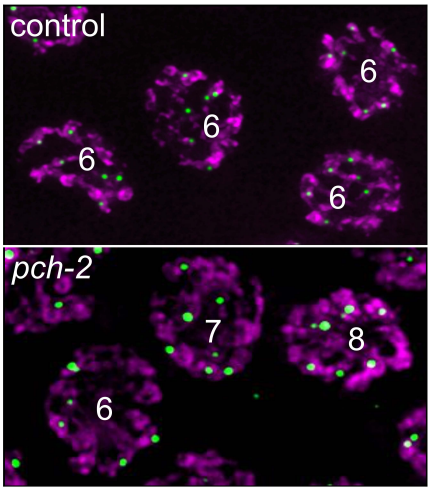
24 Hours Post Irradiation
control
6
6
6
6
pch-2
7
8
6

F

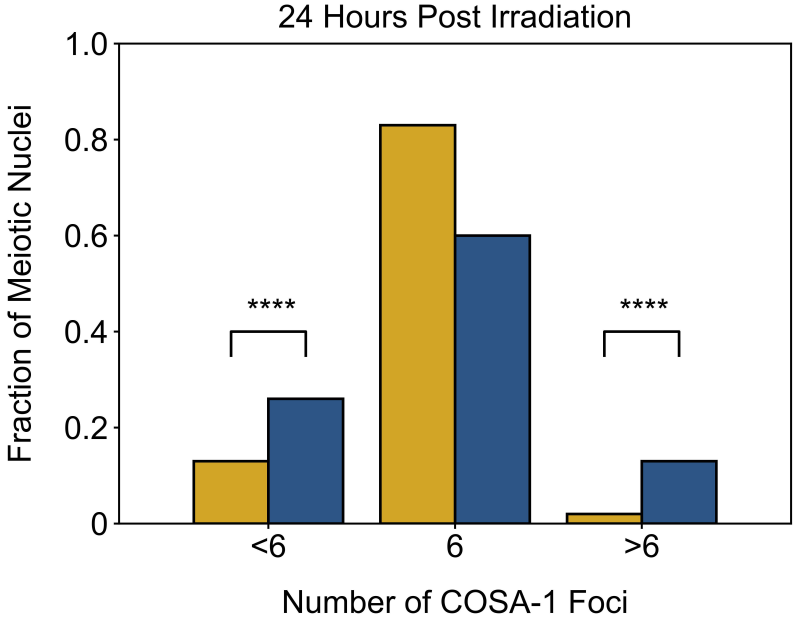
24 Hours Post Irradiation
Fraction of Meiotic Nuclei
1.0
0.8
0.6
0.4
0.2
0
****
****
<6
6
>6
Number of COSA-1 Foci

A

Areas of SPO-11 depletion to assay COSA-1 foci

Time Points
- 36 hours
- 24 hours
- 22 hours
- 20 hours
- 18 hours

B

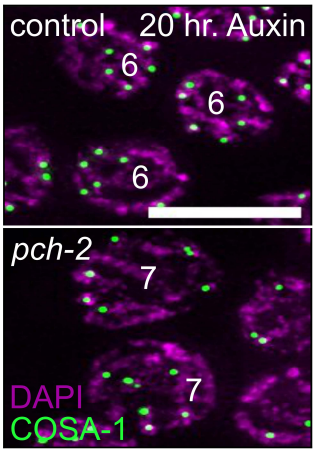

C

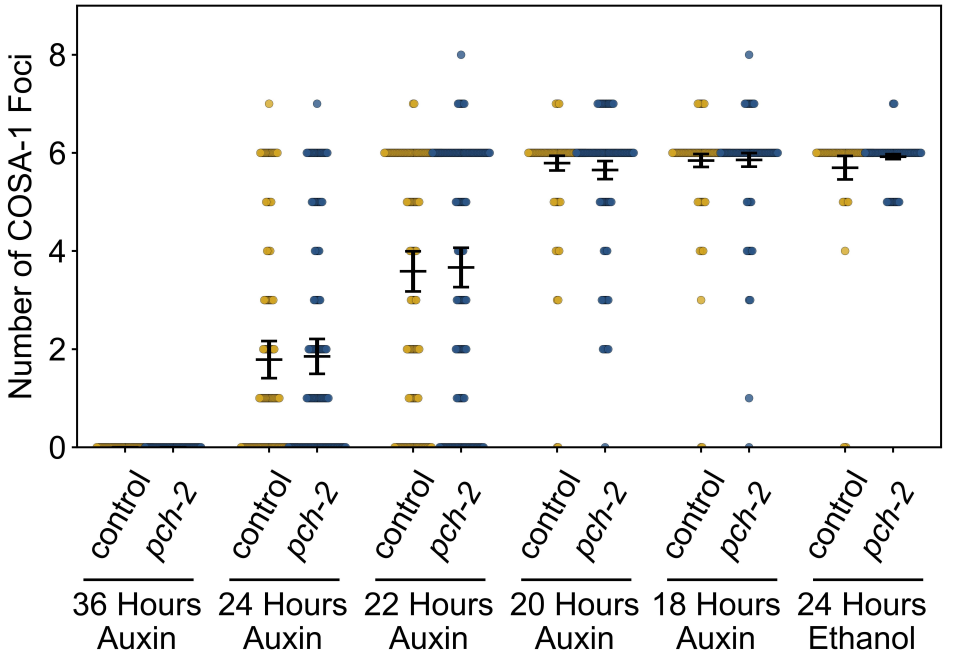

D

Areas of SPO-11 depletion to assay bivalents

Time Points
- 48 hours
- 36 hours
- 34 hours
- 32 hours
- 30 hours

E

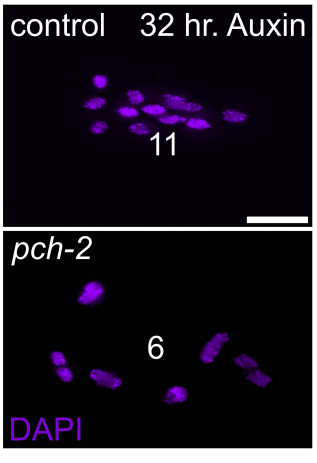

F

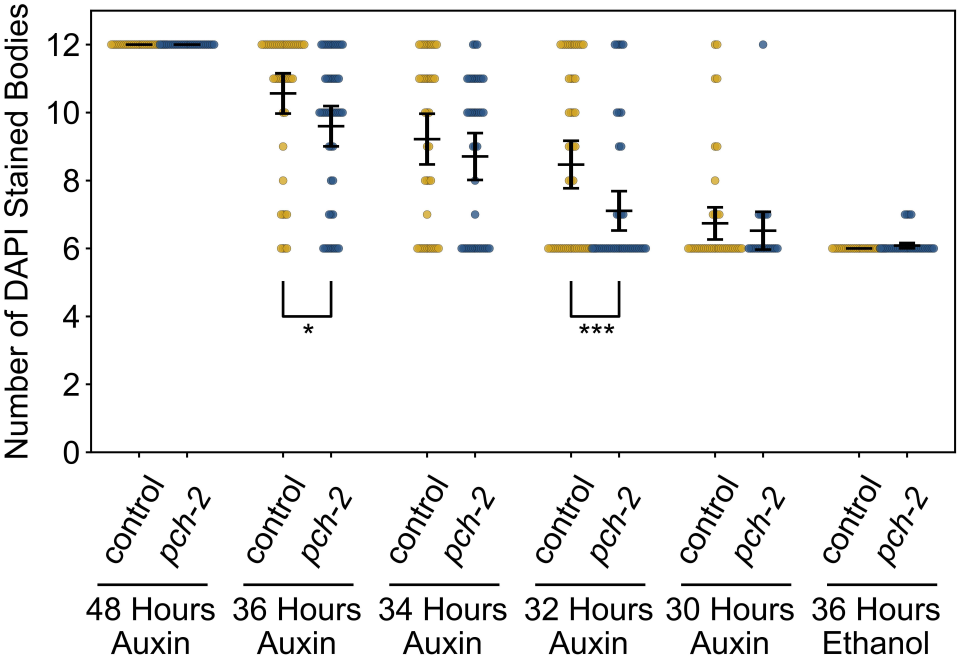

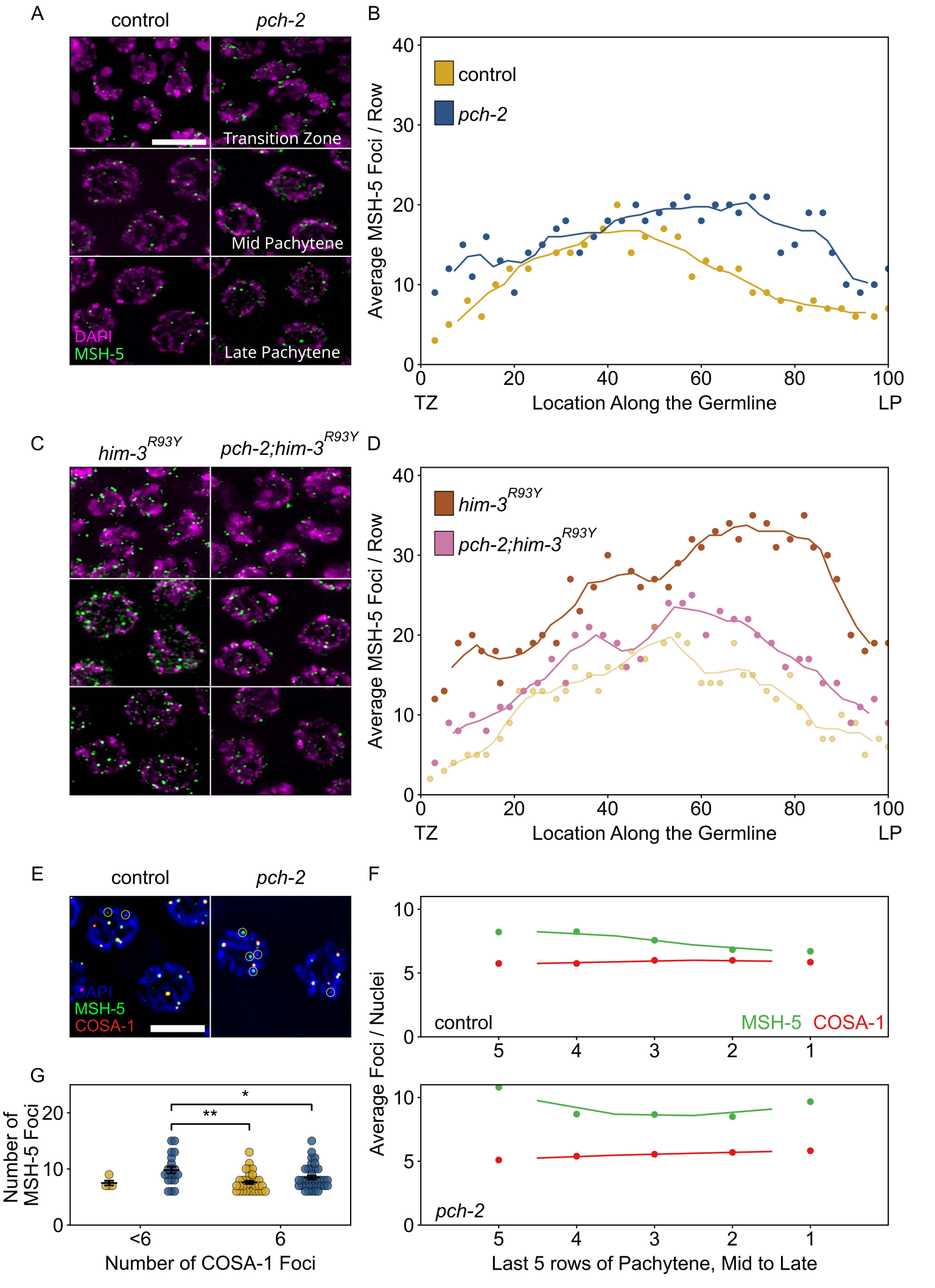
A
control
pch-2
Transition Zone
Mid Pachytene
Late Pachytene
DAPI
MSH-5
B
control
pch-2
Average MSH-5 Foci / Row
Location Along the Germline
TZ
LP
C
him-3R93Y
pch-2;him-3R93Y
D
him-3R93Y
pch-2;him-3R93Y
Average MSH-5 Foci / Row
Location Along the Germline
TZ
LP
E
control
pch-2
DAPI
MSH-5
COSA-1
F
control
MSH-5
COSA-1
pch-2
Average Foci / Nuclei
Last 5 rows of Pachytene, Mid to Late
G
Number of MSH-5 Foci
Number of COSA-1 Foci
<6
6

A

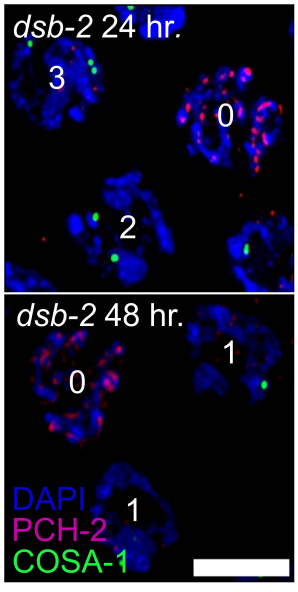
dsb-2 24 hr.
3
0
2
dsb-2 48 hr.
0
1
1
DAPI
PCH-2
COSA-1

B

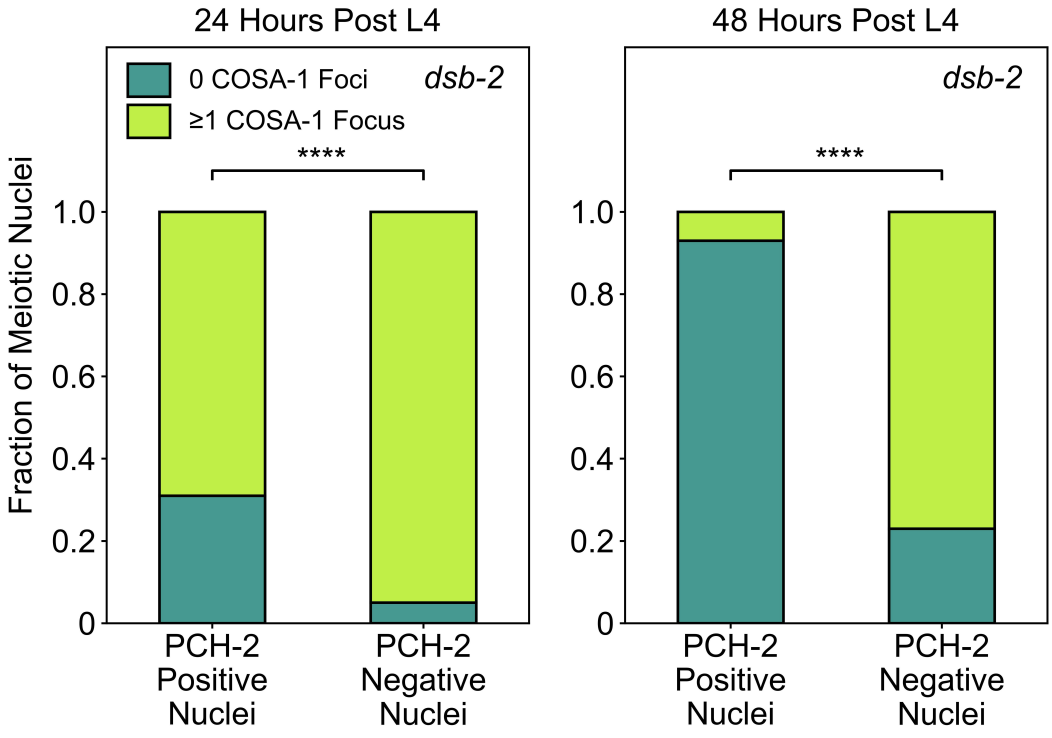
24 Hours Post L4
48 Hours Post L4
0 COSA-1 Foci
≥1 COSA-1 Focus
dsb-2
****
Fraction of Meiotic Nuclei
1.0
0.8
0.6
0.4
0.2
0
PCH-2 Positive Nuclei
PCH-2 Negative Nuclei

C

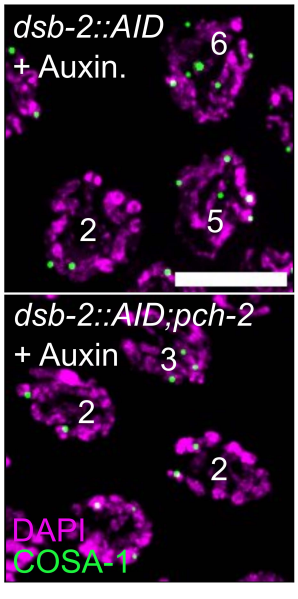
dsb-2::AID
+ Auxin.
6
2
5
dsb-2::AID;pch-2
+ Auxin
3
2
2
DAPI
COSA-1

D

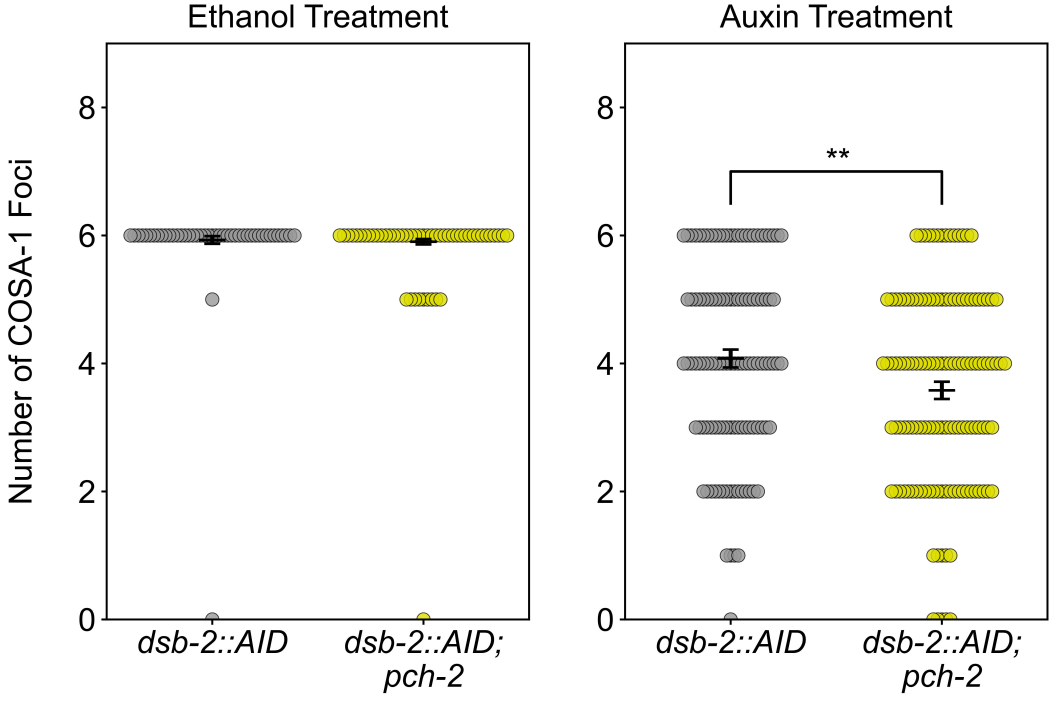
Ethanol Treatment
Auxin Treatment
Number of COSA-1 Foci
8
6
4
2
0
**
dsb-2::AID
dsb-2::AID; pch-2

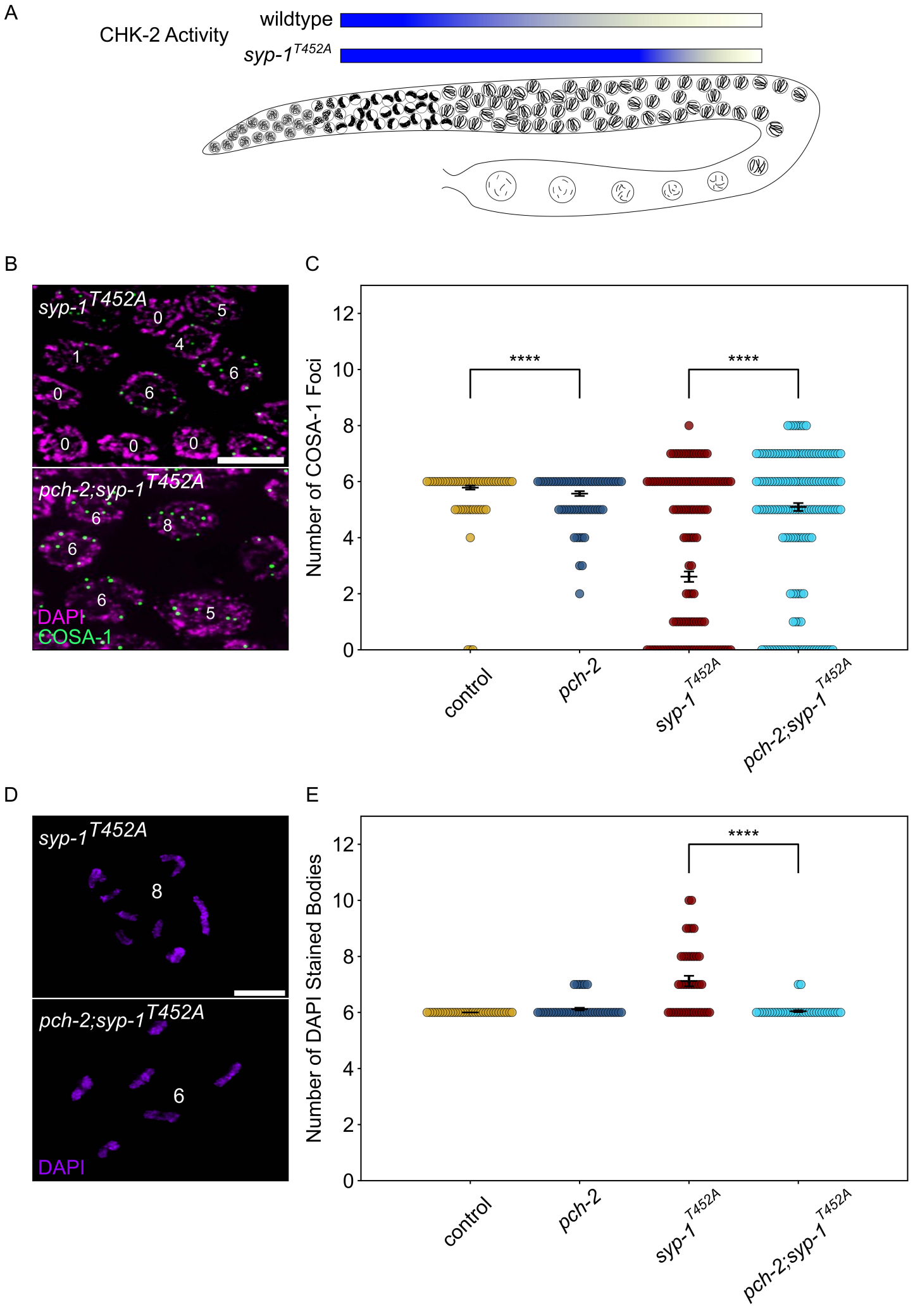
A
CHK-2 Activity
wildtype
syp-1T452A
B
syp-1T452A
pch-2;syp-1T452A
DAPI
COSA-1
C
Number of COSA-1 Foci
****
****
control
pch-2
syp-1T452A
pch-2;syp-1T452A
D
syp-1T452A
pch-2;syp-1T452A
DAPI
E
Number of DAPI Stained Bodies
****
control
pch-2
syp-1T452A
pch-2;syp-1T452A

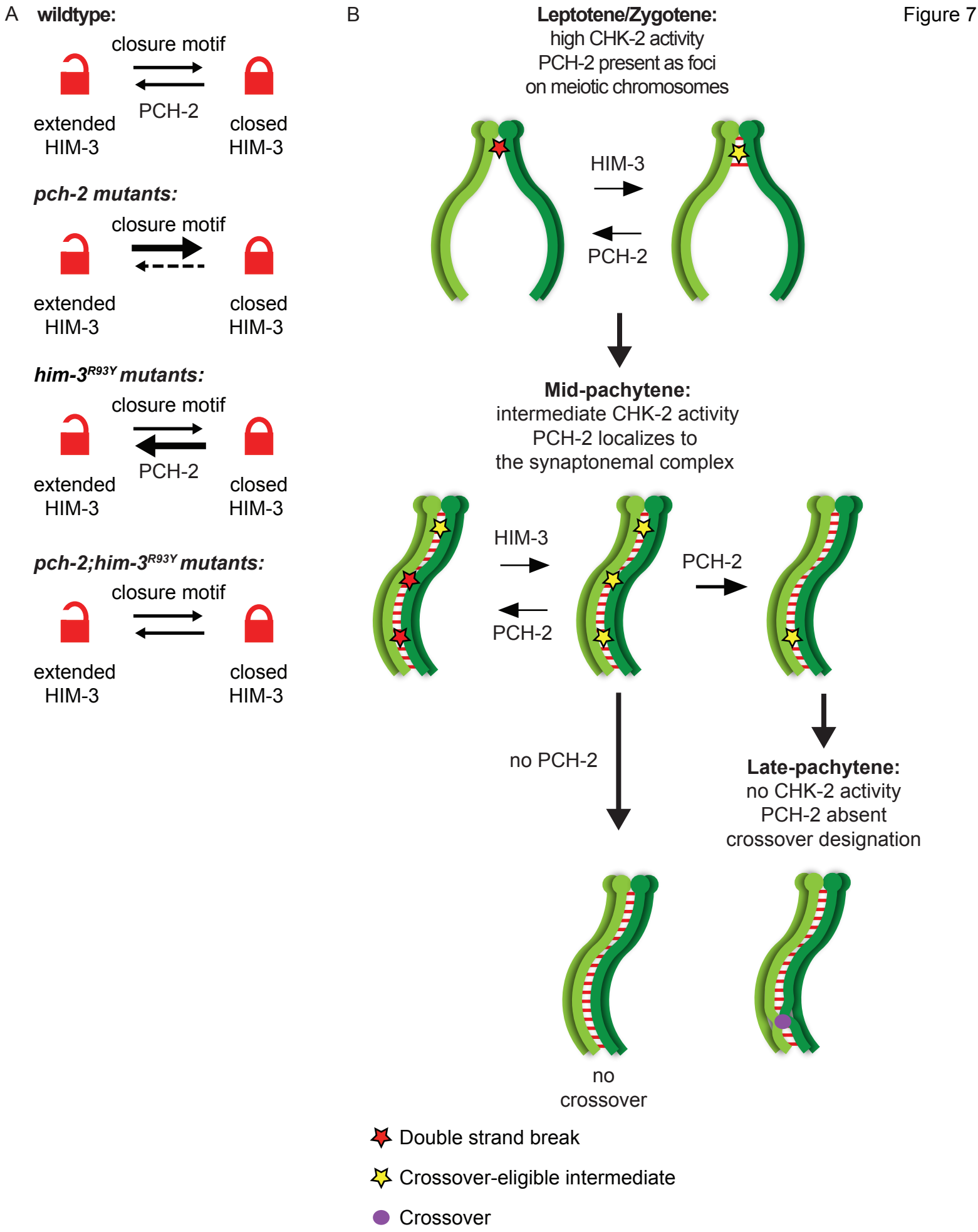
A
wildtype:
closure motif
PCH-2
extended HIM-3
closed HIM-3
pch-2 mutants:
closure motif
extended HIM-3
closed HIM-3
him-3R93Y mutants:
closure motif
PCH-2
extended HIM-3
closed HIM-3
pch-2;him-3R93Y mutants:
closure motif
extended HIM-3
closed HIM-3
B
Leptotene/Zygotene:
high CHK-2 activity
PCH-2 present as foci
on meiotic chromosomes
HIM-3
PCH-2
Mid-pachytene:
intermediate CHK-2 activity
PCH-2 localizes to
the synaptonemal complex
HIM-3
PCH-2
PCH-2
no PCH-2
Late-pachytene:
no CHK-2 activity
PCH-2 absent
crossover designation
no
crossover
Double strand break
Crossover-eligible intermediate
Crossover

Figure 7

Supplementary Table 1: Single nucleotide polymorphisms used for recombination assay

Chromosome and SNP	Primer Name	Primer Genetic Location	Primer Sequence FOR	Primer Sequence REV	Restriction enzyme	N2	HI
IA	F56C11	-19	ATGCCAGTGATAAGGAACGG	TCACATCCCTTGTCGATGAA	DraI	354, 146	500
IB	Y71G12	–12.3	GACAATGACCAATAAGACG	GATCCGTGAAATTGTTCCG	BsrI	440, 125	364, 125, 76
IC	K04F10	0.9	ATCATTCTCCAGGCCACGTTAC	CTGAACTAGTCGAACAAACCCC	NdeI	594	300, 294
ID	T07D10	13.6	CTTGGTGTGGGGAGAGTATAGG	TTTGTCCGGATTGACTCTGC	Sau3AI	303, 63	207, 96, 63
IE	ZK909	28.8	CACAAGTGGTTTGGAAGTACCG	CAACAAAGGGATAGATCACGGG	HindIII	450	236, 214
IIIA	pkP3081	-26.98	AGCAAGAATGAGCCGATTG	GTCGGCCGTTTTCAAATAACTG	TaqI	222, 149	195, 145, 27
IIIB	pkP3095	-5.12	TCTCGTCAATTGTCGCCTG	TTATTTGCAATCCAACGGC	ApoI	308	168, 140
IIIC	pkP3101	-0.9	CCAAGTGCAAACTATGGTGC	ATAAACAATTTCAGTGCCGC	HinfI	495	282, 213
IIID	pkP3035	0.9	CGTAAACTACCAAACTCGGTG	GGTCTACTACAACTATACAGGC	Eco0109I	732	419, 313
IIIE	pkP3080	21.29	CGGTGGTGGTAAAAGTGTAAC	CAACATTCAGGCTGTGCTTTCC	Hpy188III	365, 76, 68, 35	241, 124, 76, 68, 35
IVA	F56B3	-24	TGATGGTGTGTCTGCGTACC	AGAGCTGGAGAGCACGGATA	DraI	301, 128, 71	429, 71
IVB	F52C12	−14.9	ACATTTAGTCACGCGTAGGG	GCCCGAATCTAGCACATAAG	HpaII	191, 137, 22	328, 22
IVC	B0273	1.8	AATACAGCAGTCGTTCCGTTC	TGAACTTCATGAACCAGCTTG	DraI	288, 144	432

IVD	K10D11	6.7	GATTATTTCAGAGGAGCAGAGC	CATAGCACGTGGAATAACCAC	HindIII	420	245, 175
IVE	T02D1	16.8	TGCTTAAAGTCATCGTGTCCAC	TGTAAACCGTATCGAATCCGAC	EarI	174, 235	408
XA	pkP6139	-19.97	AAGAGTGAACCTTTTCCGTGAG	TGATGCAATTTATACACACGCC	MseI	401, 31	279, 122, 31
XB	pkP6120	-10.46	TCGTGGCACCATAAAAGTG	GATTCAGATCAAACAGAGGTGG	DraI	243	128, 115
XC	pkP6157	-0.14	GGGGTATAATGAACCAACCTG	TGTAGGAACCGTTTGTTTCTTC	ApoI	261, 48	150, 111, 48
XD	pkP6161	9.38	ATCGACCCCAACAATGCAC	TCCGTCATCCAAATCTCCG	AseI	542	287, 255
XE	pkP6170	24.07	CGCTGTCACAATCTCTAAAATG	AAACCCTCCCCACTTTGTTGTC	ApoI	249, 118, 56	197, 118, 56, 52

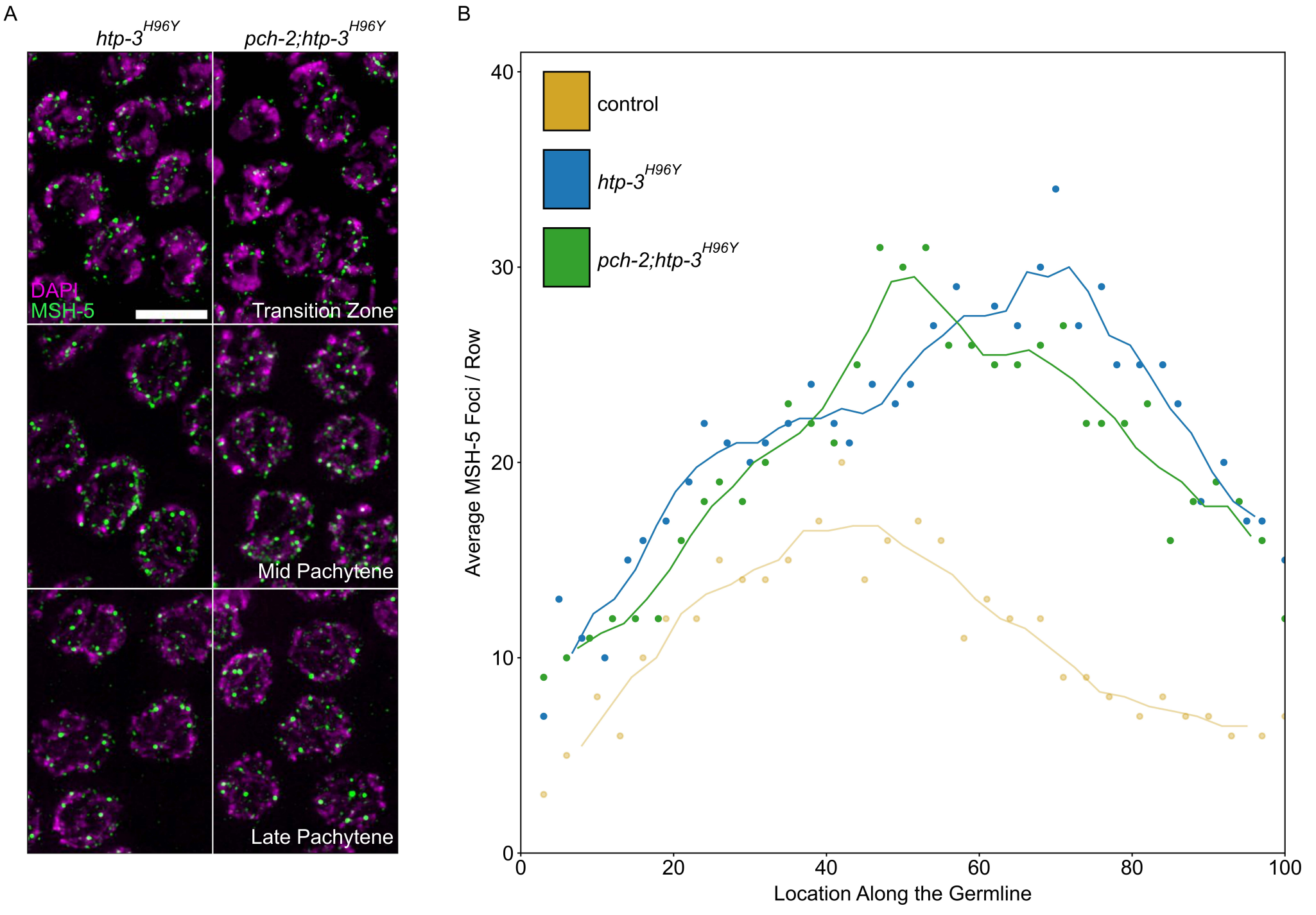
A
htp-3H96Y
pch-2;htp-3H96Y
DAPI
MSH-5
Transition Zone
Mid Pachytene
Late Pachytene
B
control
htp-3H96Y
pch-2;htp-3H96Y
Average MSH-5 Foci / Row
Location Along the Germline
0
10
20
30
40
0
20
40
60
80
100

A

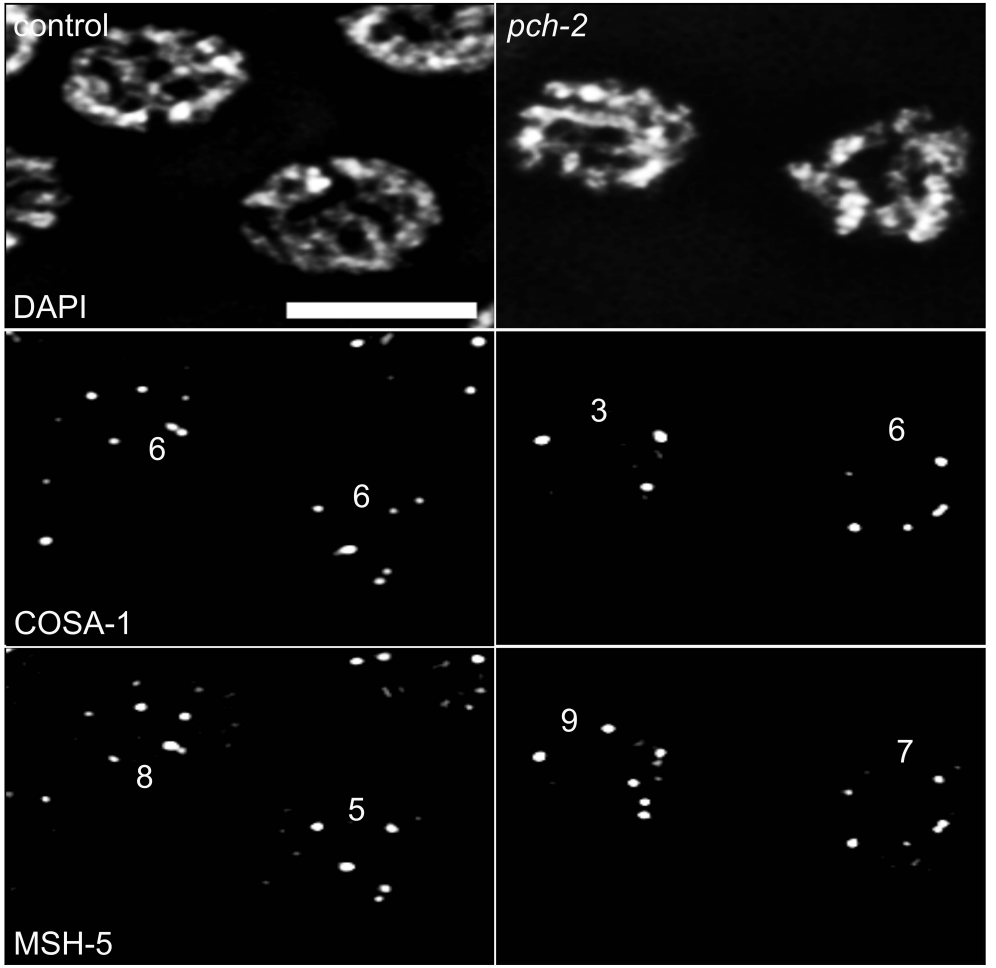

A

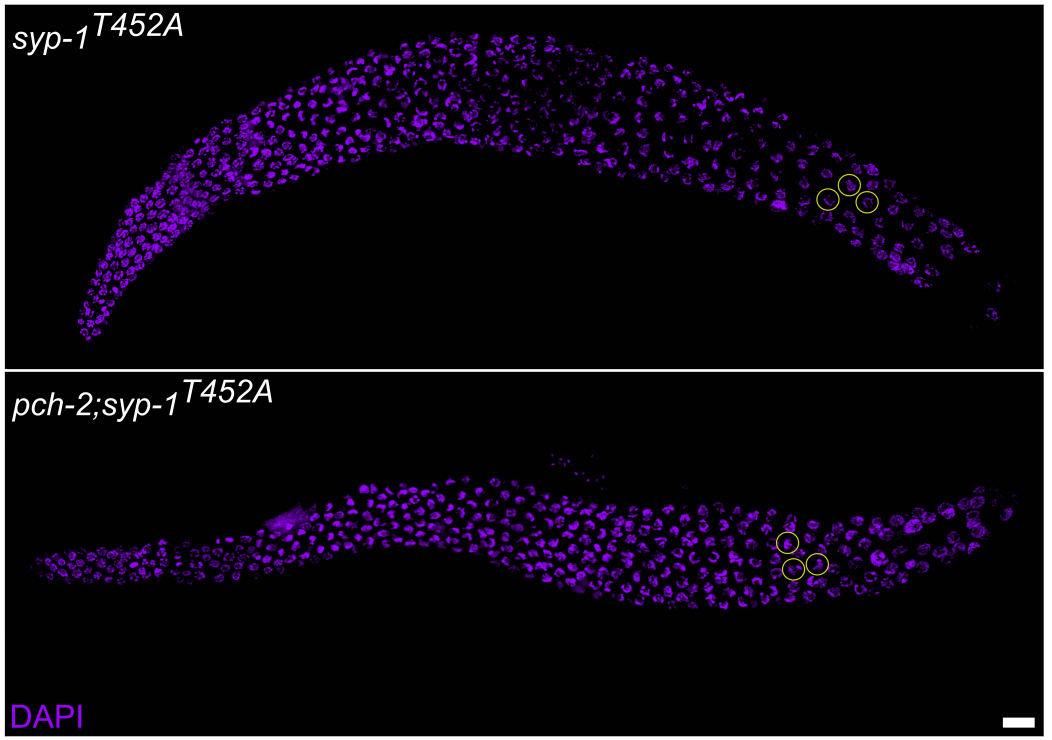
syp-1T452A
pch-2;syp-1T452A
DAPI

B

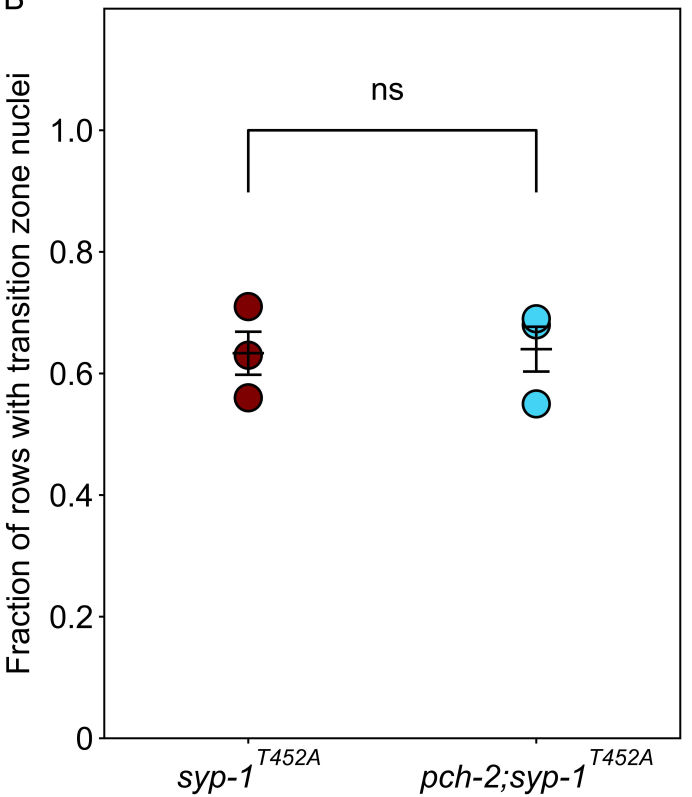
ns
Fraction of rows with transition zone nuclei
1.0
0.8
0.6
0.4
0.2
0
syp-1T452A
pch-2;syp-1T452A